Available on the CERN CDS information server **CMS PAS SUS-14-002**

CMS Physics Analysis Summary

Contact: cms-pag-conveners-susy@cern.ch 2014/07/03

Search for electroweak neutralino and chargino production in channels with Higgs, Z, and W bosons in pp collisions at 8 TeV

The CMS Collaboration

Abstract

A search for supersymmetry (SUSY) is presented based on the electroweak pair production of neutralinos and charginos, leading to decay channels with Higgs, Z, and W bosons and undetected lightest SUSY particles (LSPs). The data sample corresponds to an integrated luminosity of about 19.5 fb^{-1} of proton-proton collisions collected in 2012 by the CMS experiment at the LHC at a center-of-mass energy of 8 TeV. The main emphasis is neutralino pair production in which each neutralino decays either to a Higgs boson (h) and an LSP or to a Z boson and an LSP, leading to hh, hZ, and ZZ states with missing transverse energy ($E_{\text{T}}^{\text{miss}}$). A second aspect is chargino-neutralino pair production, leading to hW states with $E_{\text{T}}^{\text{miss}}$. The decays of a Higgs boson to a bottom-quark pair, to a photon pair, and to final states with leptons are considered in conjunction with hadronic and leptonic decay modes of the Z and W bosons. No evidence is found for supersymmetric interactions, and 95% confidence level upper limits are evaluated for the respective pair production cross sections and for neutralino and chargino mass values.

1 Introduction

Supersymmetry (SUSY) [1–8], one of the most widely considered extensions of the standard model (SM) of particle physics, predicts unification of the strong, weak, and electromagnetic forces, stabilizes the calculation of the Higgs boson mass at the electroweak energy scale, and may provide a dark matter candidate. SUSY postulates that each SM particle is paired with a SUSY partner from which it differs in spin by one-half unit, with otherwise identical quantum numbers. For example, squarks, gluinos, and winos are the SUSY partners of quarks, gluons, and W bosons, respectively. SUSY models contain extended Higgs sectors [8, 9], with higgsinos the SUSY partners of Higgs bosons. Neutralinos $\widetilde{\chi}^0$ (charginos $\widetilde{\chi}^{\pm}$) arise from the mixture of neutral (charged) higgsinos with the SUSY partners of neutral (charged) electroweak vector bosons.

In R-parity-conserving models [10], SUSY particles are created in pairs. Each member of the pair initiates a decay chain that terminates with a stable lightest SUSY particle (LSP) and SM particles. If the LSP interactions are weak only, as in the case of a dark matter candidate, the LSP escapes detection, potentially yielding large values of missing transverse energy $E_{\mathrm{T}}^{\mathrm{miss}}$.

Extensive searches for SUSY particles have been performed at the Large Hadron Collider (LHC) at CERN, but so far without uncovering evidence for their existence [11–22]. The recent discovery [23–25] of a Higgs boson with a mass of about 125 GeV opens new possibilities for SUSY searches. In the SUSY context, we refer to the 125 GeV boson as "h" [26], the lightest neutral CP-even state of extended Higgs sectors. The h boson is expected to have SM Higgs boson properties if all other Higgs bosons are much heavier [27]. Neutralinos and charginos are predicted to decay to an h or vector (V) boson over large regions of SUSY parameter space [28–34], with V a Z or W boson. Pair production of neutralinos and/or charginos can thus lead to hh, hV, and $\mathrm{VV}^{(\prime)}$ states. Requiring the presence of one or more h bosons provides a novel means to search for these channels. Furthermore, the observation of a Higgs boson in a SUSY-like process would provide evidence that SUSY particles couple to the Higgs field, a necessary condition for SUSY to stabilize the Higgs boson mass calculation. This evidence is not provided by search channels without a Higgs boson.

In this paper, searches are presented for the electroweak pair production of neutralinos and charginos that decay to yield hh, hZ, and hW states. Related SUSY searches sensitive to the corresponding ZZ state are presented in Refs. [35, 36]. We assume the Higgs boson h to have SM properties. The data, corresponding to an integrated luminosity of around $19.5\,\mathrm{fb}^{-1}$ of proton-proton collisions at $\sqrt{s} = 8\,\mathrm{TeV}$, were collected with the Compact Muon Solenoid (CMS) detector at the LHC. For most of the searches, large values of $E_{\mathrm{T}}^{\mathrm{miss}}$ are required.

The hh, hZ, and ZZ topologies arise in a number of SUSY scenarios. As a specific example, we consider an R-parity-conserving gauge-mediated SUSY-breaking (GMSB) model [28, 34] in which the two lightest neutralinos $\widetilde{\chi}_1^0$ and $\widetilde{\chi}_2^0$ and the lightest chargino $\widetilde{\chi}_1^{\pm}$ are higgsinos. In this model, the $\widetilde{\chi}_1^0$, $\widetilde{\chi}_2^0$ and $\widetilde{\chi}_1^{\pm}$ are approximately mass-degenerate, with $\widetilde{\chi}_1^0$ the lightest of the three states. The LSP is a gravitino $\widetilde{\mathrm{G}}$ [37], the SUSY partner of a graviton. The $\widetilde{\chi}_2^0$ and $\widetilde{\chi}_1^{\pm}$ higgsinos decay to the $\widetilde{\chi}_1^0$ state plus low-p_{T} SM particles, where p_{T} represents momentum transverse to the beam axis. The $\widetilde{\chi}_1^0$ higgsino, which is the next-to-lightest SUSY particle (NLSP), undergoes two-body decay to either an h boson and $\widetilde{\mathrm{G}}$ or to a Z boson and $\widetilde{\mathrm{G}}$, where $\widetilde{\mathrm{G}}$ is nearly massless, stable, and weakly interacting. The pair production of any of the combinations $\widetilde{\chi}_1^0\widetilde{\chi}_2^0$, $\widetilde{\chi}_1^0\widetilde{\chi}_1^{\pm}$, $\widetilde{\chi}_2^0\widetilde{\chi}_1^{\pm}$, or $\widetilde{\chi}_1^{\pm}\widetilde{\chi}_1^{\pm}$ is allowed, enhancing the effective cross section for the $\widetilde{\chi}_1^0\widetilde{\chi}_1^0$ di-higgsino state and thus for hh and hZ production (Fig. 1 left and center). The production of ZZ combinations is also possible. The final state includes two LSP particles $\widetilde{\mathrm{G}}$, leading to $E_{\mathrm{T}}^{\mathrm{miss}}$.

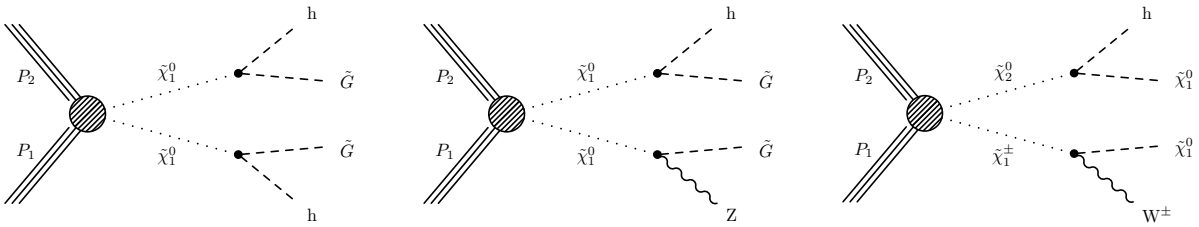

Figure 1: Event diagrams for the SUSY scenarios considered in this analysis. (left and center) hh and hZ production in a GMSB model [28, 34], with h a Higgs boson, $\widetilde{\chi}_1^0$ a lightest neutralino NLSP, and $\widetilde{G}$ is a nearly massless gravitino LSP. The $\widetilde{\chi}_1^0\widetilde{\chi}_1^0$ state is created through $\widetilde{\chi}_1^0\widetilde{\chi}_2^0$, $\widetilde{\chi}_1^0\widetilde{\chi}_1^\pm$, $\widetilde{\chi}_2^0\widetilde{\chi}_1^\pm$, and $\widetilde{\chi}_1^\pm\widetilde{\chi}_1^\pm$ production followed by the decay of the $\widetilde{\chi}_2^0$ and $\widetilde{\chi}_1^\pm$ states to the $\widetilde{\chi}_1^0$ and undetected SM particles, with $\widetilde{\chi}_2^0$ and $\widetilde{\chi}_1^\pm$ the second-lightest neutralino and the lightest chargino, respectively. (right) hW production through chargino-neutralino $\widetilde{\chi}_1^\pm\widetilde{\chi}_2^0$ pair creation, with $\widetilde{\chi}_1^0$ a massive neutralino LSP.

For the hh combination, we consider the $\mathrm{h}(\to \mathrm{b\bar{b}})\mathrm{h}(\to \mathrm{b\bar{b}})$, the $\mathrm{h}(\to \gamma\gamma)\mathrm{h}(\to \mathrm{b\bar{b}})$, and the $\mathrm{h}(\to \gamma\gamma)\mathrm{h}(\to \mathrm{ZZ/WW}/\tau\tau)$ decay channels, with $\mathrm{b\bar{b}}$ a bottom quark-antiquark pair and where the ZZ, WW, and $\tau\tau$ states decay to yield at least one electron or muon. For the hZ combination, we consider the $\mathrm{h}(\to \gamma\gamma)\mathrm{Z}(\to 2\text{ jets})$, $\mathrm{h}(\to \gamma\gamma)\mathrm{Z}(\to \mathrm{ee}/\mu\mu/\tau\tau)$, and $\mathrm{h}(\to \mathrm{b\bar{b}})\mathrm{Z}(\to \mathrm{ee}/\mu\mu)$ channels, where the $\tau\tau$ pair yields at least one electron or muon. We combine the results of the current study with those presented for complementary Higgs and Z boson decay modes in Refs. [35, 36] to derive unified conclusions for electroweak GMSB hh, hZ, and ZZ production.

As a second specific example of a SUSY scenario with Higgs bosons, we consider the R-parity-conserving chargino-neutralino $\widetilde{\chi}_1^\pm\widetilde{\chi}_2^0$ electroweak pair-production process shown in Fig. 1 (right), in which the $\widetilde{\chi}_1^\pm$ chargino is wino-like and the $\widetilde{\chi}_1^0$ neutralino is a massive, stable, weakly interacting LSP. This scenario represents the SUSY process with the largest electroweak cross section [38]. It leads to the hW topology, with $E_\mathrm{T}^\mathrm{miss}$ present because of the two LSP particles. The decay channels considered are $\mathrm{h}(\to \gamma\gamma)\mathrm{W}(\to 2\text{ jets})$ and $\mathrm{h}(\to \gamma\gamma)\mathrm{W}(\to \ell\nu)$, with ℓ an electron, muon, or leptonically decaying τ lepton. We combine these results with those based on complementary decay modes of this same scenario [36] to derive unified conclusions.

The principal backgrounds arise from the production of a top-quark-antiquark ($\mathrm{t\bar{t}}$) pair, a W boson, Z boson, or photon in association with jets (W+jets, Z+jets, and γ+jets), and multiple jets through the strong interaction (QCD multijet). Other backgrounds are due to events with a single-top quark or that include rare processes such as $\mathrm{t\bar{t}V}$ or $\mathrm{t\bar{t}h}$ combinations. The QCD multijet category excludes events in the other categories. For events with a top quark or W boson, significant $E_\mathrm{T}^\mathrm{miss}$ can arise if a W boson decays leptonically, producing a neutrino, while for events with a Z boson, the decay of the Z boson to two neutrinos can yield significant $E_\mathrm{T}^\mathrm{miss}$. For γ+jets events, Z+jets events with $\mathrm{Z} \to \ell^+\ell^-$ ($\ell = \mathrm{e}, \mu$), and events with all-hadronic final states such as QCD multijet events, significant $E_\mathrm{T}^\mathrm{miss}$ can arise if the event contains a charm or bottom quark that undergoes semileptonic decay, but the principal source of $E_\mathrm{T}^\mathrm{miss}$ is due to the mismeasurement of jet p_T.

This paper is organized as follows. In Sections 2, 3, and 4, we discuss the detector and trigger, the event reconstruction, and the event simulation. Section 5 presents a search for hh SUSY events in which both Higgs bosons decay to a $\mathrm{b\bar{b}}$ pair. Section 6 presents searches for hh, hZ, and hW SUSY events in which one Higgs boson decays to a diphoton state. A search for hZ SUSY events with a Higgs boson that decays to a $\mathrm{b\bar{b}}$ pair and a Z boson that decays to an $\mathrm{e^+e^-}$ or $\mu^+\mu^-$ pair is presented in Section 7. In Section 8, we briefly discuss the studies of

Refs. [35, 36] as they pertain to the SUSY scenarios considered here. The interpretation of the results is presented in Section 10 and a summary in Section 11.

2 Detector and trigger

A detailed description of the CMS detector is given elsewhere [39]. A superconducting solenoid of 6 m internal diameter provides an axial magnetic field of 3.8 T. Within the field volume are a silicon pixel and strip tracker, a crystal electromagnetic calorimeter, and a brass-and-scintillator hadron calorimeter. Muon detectors based on gas ionization chambers are embedded in a steel flux-return yoke located outside the solenoid. The CMS coordinate system is defined with the origin at the center of the detector and with the z axis along the direction of the counterclockwise beam. The transverse plane is perpendicular to the beam axis, with ϕ the azimuthal angle (measured in radians), θ the polar angle, and $\eta = -\ln[\tan(\theta/2)]$ the pseudorapidity. The tracking system covers the region $|\eta| < 2.5$, the muon detector $|\eta| < 2.4$, and the calorimeters $|\eta| < 3.0$. Steel-and-quartz-fiber forward calorimeters cover $3 < |\eta| < 5$. The near-hermeticity of the detector permits accurate measurements of energy balance in the transverse plane.

The trigger is based on the identification of events with one or more jets, bottom-quark jets (b jets), photons, or charged leptons. The main trigger used for the $\mathrm{hh} \to \mathrm{b\bar{b}b\bar{b}}$ analysis (Section 5) requires the presence of at least two jets with $p_{\mathrm{T}} > 30\,\mathrm{GeV}$, including at least one tagged b jet, and $E_{\mathrm{T}}^{\mathrm{miss}} > 80\,\mathrm{GeV}$. For the diphoton studies (Section 6), there must be at least one photon with $p_{\mathrm{T}} > 36\,\mathrm{GeV}$ and another with $p_{\mathrm{T}} > 22\,\mathrm{GeV}$. The study utilizing $\mathrm{Z} \to \ell^{+}\ell^{-}$ events (Section 7) requires at least one electron or muon with $p_{\mathrm{T}} > 17\,\mathrm{GeV}$ and another with $p_{\mathrm{T}} > 8\,\mathrm{GeV}$. Corrections are applied to the selection efficiencies to account for trigger inefficiencies.

3 Event reconstruction

The particle-flow (PF) method [40, 41] is used to reconstruct and identify charged and neutral hadrons, electrons (with associated bremsstrahlung photons), muons, and photons, using an optimized combination of information from CMS subdetectors. The reconstruction of photons for the $\mathrm{h} \to \gamma\gamma$-based searches is discussed in Section 6. Hadronically decaying τ leptons are reconstructed using PF objects (we use the "hadron-plus-strips" τ-lepton reconstruction algorithm [42] with loose identification requirements). The event primary vertex, taken to be the reconstructed vertex with the largest sum of charged-track p_{T}^2 values, is required to contain at least four charged tracks and to lie within 24 cm of the origin in the direction along the beam axis and 2 cm in the perpendicular direction. The PF objects serve as input for jet reconstruction, based on the anti-k_{T} algorithm [43, 44], with a distance parameter of 0.5. Jet corrections are applied as a function of p_{T} and η to account for residual effects of non-uniform detector response. Contributions to an individual jet's p_{T} from extraneous pp interactions within the same or a nearby bunch crossing ("pileup") are subtracted using the jet area method described in Ref. [45]. Jets from pileup interactions are suppressed through requirements on the compatibility of the jet's charged particle constituents with the primary vertex. Jets are required to satisfy basic quality criteria (jet ID), which eliminate, for example, spurious events caused by calorimeter noise.

The missing transverse energy $E_{\mathrm{T}}^{\mathrm{miss}}$ is defined as the modulus of the vector sum of the transverse momenta of all PF objects. The $E_{\mathrm{T}}^{\mathrm{miss}}$ vector is the negative of that same vector sum. We also make use of the $E_{\mathrm{T}}^{\mathrm{miss}}$-significance variable $\mathcal{S}_{\mathrm{MET}}$ [46], which represents a χ^2 difference between the observed result for $E_{\mathrm{T}}^{\mathrm{miss}}$ and the $E_{\mathrm{T}}^{\mathrm{miss}} = 0$ hypothesis. Because it accounts for finite jet resolution on an event-by-event basis, $\mathcal{S}_{\mathrm{MET}}$ provides better discrimination between

signal and background events than does $E_{\mathrm{T}}^{\mathrm{miss}}$ for background events with $E_{\mathrm{T}}^{\mathrm{miss}}$ due to jet p_{T} mismeasurements.

The identification of b jets is performed using the combined secondary vertex (CSV) algorithm [47, 48], which computes a discriminating variable for each jet based on displaced secondary vertices, tracks with large impact parameters, and kinematical variables like jet mass. Three operating points are defined, denoted "loose," "medium," and "tight." These three working points yield average signal efficiencies for b jets (misidentification probabilities for light-parton jets) of approximately 83% (10%), 70% (1.5%), and 55% (0.1%), respectively, for jet p_{T} values above 60 GeV, as determined from multijet and $\mathrm{t\bar{t}}$ event samples.

We also make use of isolated electrons and muons, either vetoing events with such leptons in order to reduce background from SM $\mathrm{t\bar{t}}$ and electroweak boson production (Sections 5, 6.1, and 6.2), or selecting these events because they correspond to the targeted signal process (Sections 6.3 and 7). Isolated electron and muon identification is based on the variable R_{iso}, which is the scalar sum of the p_{T} values of charged hadrons, neutral hadrons, and photons within a cone of radius $R_{\mathrm{cone}} \equiv \sqrt{(\Delta\phi)^2 + (\Delta\eta)^2}$ around the lepton direction, divided by the lepton p_{T} value itself. For the analyses presented here, $R_{\mathrm{cone}} = 0.3$ for electrons, and $R_{\mathrm{cone}} = 0.4$ for muons unless otherwise stated.

4 Event simulation

Monte Carlo (MC) simulations of signal and background processes are used to optimize selection criteria, validate analysis performance, determine signal efficiencies, and evaluate some backgrounds and systematic uncertainties.

SM background events are simulated with the MADGRAPH 5.1.3.30 [49], POWHEG 301 [50], and PYTHIA 6.4.26 [51] generators. The SM processes are normalized to cross section calculations valid to the next-to-leading (NLO) or next-to-next-to-leading order [52–58], depending on availability, and otherwise to leading order. For the simulation of SM events, the GEANT4 [59] package is used to model the detector and detector response.

Signal events are simulated with the MADGRAPH 5.1.5.4 generator, with a Higgs boson mass of 126 GeV [60]. Up to two partons from initial-state radiation are allowed. To reduce computational requirements, the detector and detector response for signal events are modeled with the CMS fast simulation program [61], with the exception of the signal events for the $\mathrm{hh} \to \mathrm{b\bar{b}b\bar{b}}$ study (Section 5), for which GEANT4 modeling is used. The signal event rates are normalized to the NLO+NLL [38, 62, 63] cross sections for the GMSB hh, hZ, and ZZ channels, and to the NLO cross sections [38, 64] for the electroweak hW channel, where NLL is the next-to-leading-logarithmic approximation. For the GMSB scenarios [Fig. 1 (left) and (center)], the $\widetilde{\chi}_1^0$, $\widetilde{\chi}_2^0$, and $\widetilde{\chi}_1^{\pm}$ particles are taken to be mass-degenerate pure higgsino states, such that any SM particles arising from the decays of the $\widetilde{\chi}_2^0$ and $\widetilde{\chi}_1^{\pm}$ states to the $\widetilde{\chi}_1^0$ state are too soft to be detected. Signal MC samples are generated for a range of higgsino mass values $\mathrm{m}_{\widetilde{\chi}_1^0}$, taking the LSP (gravitino $\widetilde{\mathrm{G}}$) mass to be 1 GeV (i.e., effectively zero). The decays of the $\widetilde{\chi}_1^0$ higgsinos are described with a pure phase-space matrix element. For the electroweak hW scenario [Fig. 1 (right)], we make the simplifying assumption $m_{\widetilde{\chi}_2^0} = m_{\widetilde{\chi}_1^{\pm}}$ [36] and generate event samples for a range of $\widetilde{\chi}_2^0$ and LSP ($\widetilde{\chi}_1^0$) mass values, with the decays of the $\widetilde{\chi}_1^{\pm}$ chargino and $\widetilde{\chi}_2^0$ neutralino described using the BRIDGE v2.24 program [65].

All MC samples incorporate the CTEQ6L1 or CTEQ6M [66, 67] parton distribution functions, with PYTHIA used for parton showering and hadronization. The MC distributions are corrected

to account for pileup interactions, as observed in data. The simulations are further adjusted so that the b-jet tagging and misidentification efficiencies match those determined from control samples in the data. (The b-jet tagging efficiency correction factor depends slightly on jet p_T and has a typical value of 0.95 [47].) In addition, corrections are applied so that the jet energy resolution in signal samples corresponds to the observed results. A further correction, implemented as described in Appendix B of Ref. [18], accounts for mismodeling of initial-state radiation in signal events.

5 Search in the $\mathrm{hh} \to \mathrm{b\bar{b}b\bar{b}}$ channel

With a branching fraction of about 0.56 [68], $\mathrm{h} \to \mathrm{b\bar{b}}$ decays represent the most likely decay mode of the Higgs boson. The $\mathrm{h}(\to \mathrm{b\bar{b}})\mathrm{h}(\to \mathrm{b\bar{b}})$ configuration thus provides a sensitive search channel for SUSY hh production. For this channel, the principal visible objects are the four b jets. Additional jets may arise from initial-state radiation, final-state radiation, or pileup interactions. For this search, jets (including b jets) must satisfy $p_T > 20\,\mathrm{GeV}$ and $|\eta| < 2.4$. In addition, we require:

- exactly four or exactly five jets, where $p_T > 50\,\mathrm{GeV}$ for the two highest p_T jets;
- E_T^{miss} significance $\mathcal{S}_{\mathrm{MET}} > 30$;
- no identified, isolated electron or muon candidate with $p_T > 10\,\mathrm{GeV}$; electron candidates are restricted to $|\eta| < 2.5$ and muon candidates to $|\eta| < 2.4$; the isolation requirements are $R_{\mathrm{iso}} < 0.15$ for electrons and $R_{\mathrm{iso}} < 0.20$ for muons;
- no hadronically decaying τ lepton candidate with $p_T > 20\,\mathrm{GeV}$ and $|\eta| < 2.4$;
- no isolated charged particle with $p_T > 10\,\mathrm{GeV}$ and $|\eta| < 2.4$, where the isolation condition is based on the same definition of R_{iso} as given in Section 3 for electrons but using charged particle information only; we require $R_{\mathrm{iso}} < 0.10$;
- $\Delta\phi_{\mathrm{min}} > 0.5$ for events with $30 < \mathcal{S}_{\mathrm{MET}} < 50$ and $\Delta\phi_{\mathrm{min}} > 0.3$ for $\mathcal{S}_{\mathrm{MET}} > 50$, where $\Delta\phi_{\mathrm{min}}$ is the smallest difference in ϕ between the E_T^{miss} vector and any jet in the event; for the $\Delta\phi_{\mathrm{min}}$ calculation we use less restrictive criteria for jets compared with the standard criteria: $|\eta| < 5.0$, no rejection of jets from pileup interactions, and no jet ID requirements, with all other conditions unchanged.

The isolated charged particle requirement rejects events with a single-prong τ lepton or an isolated electron or muon in cases where the lepton is not identified. The $\Delta\phi_{\mathrm{min}}$ restriction eliminates QCD multijet and all-hadronic $\mathrm{t\bar{t}}$ events, whose contribution is expected to be large at small values of $\mathcal{S}_{\mathrm{MET}}$. The use of less restrictive jet requirements for the $\Delta\phi_{\mathrm{min}}$ calculation yields more efficient rejection of these backgrounds.

Three mutually exclusive samples of events with tagged b jets are defined:

- 2b sample: Events in this sample must contain exactly two tight b jets and no medium b jets;
- 3b sample: Events in this sample must contain two jets that are tight b jets, a third jet that is either a tight or a medium b jet, and no other tight, medium, or loose b jet;
- 4b sample: Events in this sample must contain two jets that are tight b jets, a third jet that is either a tight or medium b jet, and a fourth jet that is either a tight, medium, or loose b jet.

The sample most sensitive to signal events is the 4b sample. The 3b sample is included to improve signal efficiency. The 2b sample is depleted in signal events and is used to help evaluate

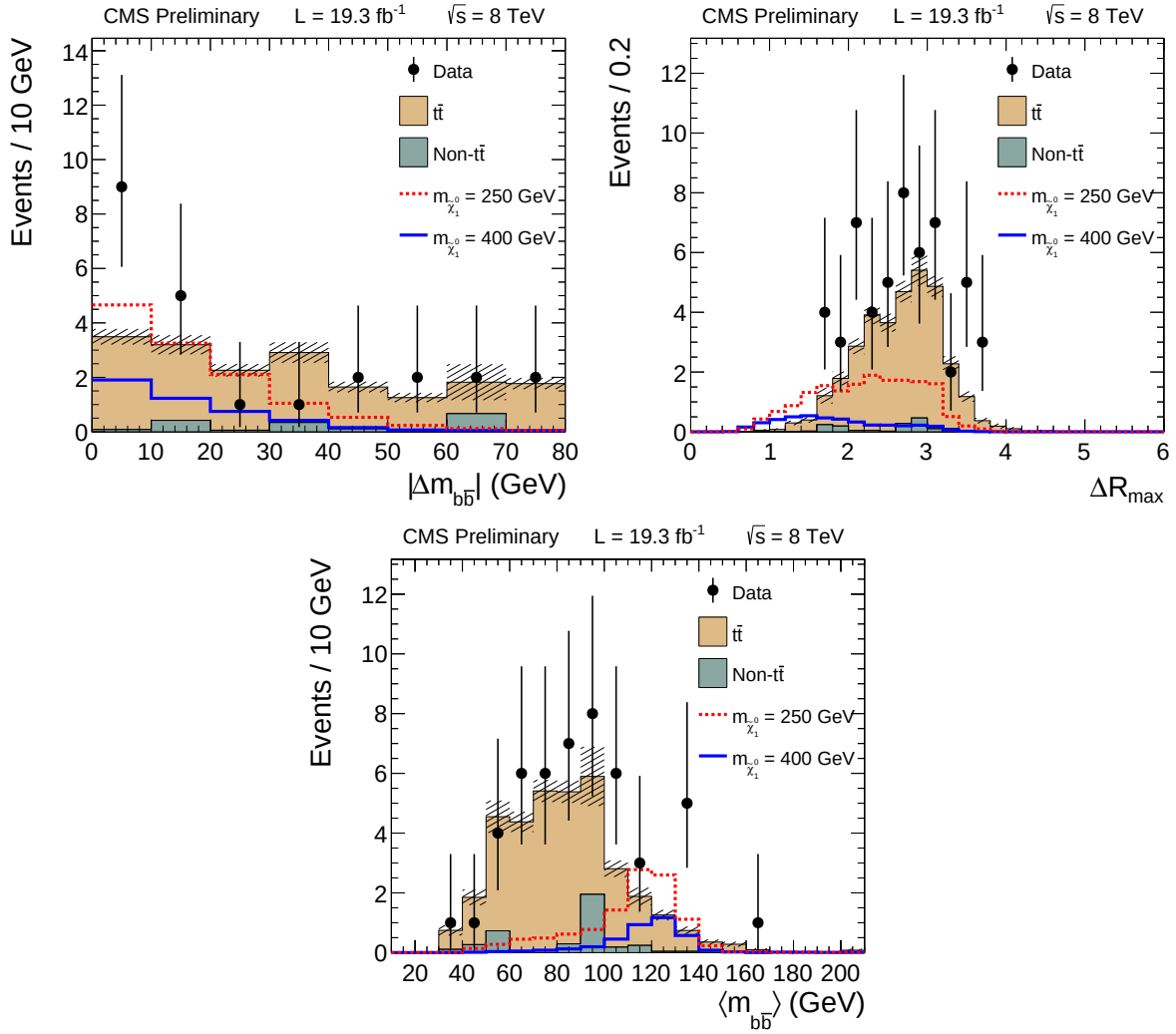

Figure 2: Distributions of events in the 4b sample of the hh → bb̄bb̄ analysis, after all signal-region requirements are applied except for that on the displayed variable, in comparison with simulations of background and signal events: (top left) $|\Delta m_{\mathrm{b\bar{b}}}|$, (top right) ΔR_{max}, and (bottom) $\langle m_{\mathrm{b\bar{b}}} \rangle$. For the signal events, results are shown for $\tilde{\chi}_1^0$ higgsino mass values of 250 and 400 GeV, with an LSP (gravitino) mass of 1 GeV. The background distributions are stacked while the signal distributions are not. The hatched bands indicate the statistical uncertainty of the total SM simulated prediction.

the background, as described below. The dominant background arises from tt̄ events in which one top quark decays hadronically while the other decays to a state with a lepton ℓ through $\mathrm{t} \to \mathrm{b}\ell\nu$, where the lepton is not identified and the neutrino provides a source of genuine $E_{\mathrm{T}}^{\mathrm{miss}}$.

To reconstruct the two Higgs boson candidates in an event, we choose the four most b-like jets based on the value of the CSV discriminating variable. These four jets can be grouped into three different pairs of Higgs boson candidates. Of the three possibilities, we choose the one with the smallest difference $|\Delta m_{\mathrm{b\bar{b}}}| \equiv |m_{\mathrm{b\bar{b}},1} - m_{\mathrm{b\bar{b}},2}|$ between the two candidate masses, where $m_{\mathrm{b\bar{b}}}$ is the invariant mass of two tagged b jets. We calculate the distance $\Delta R \equiv \sqrt{(\Delta\phi)^2 + (\Delta\eta)^2}$ between the two jets for each $\mathrm{h} \to \mathrm{b\bar{b}}$ candidate. We call the larger of these two values ΔR_{max}. In signal events, the two b jets from the decay of a Higgs boson generally have similar directions. Thus the two ΔR values tend to be small, making ΔR_{max} small. In contrast, for the

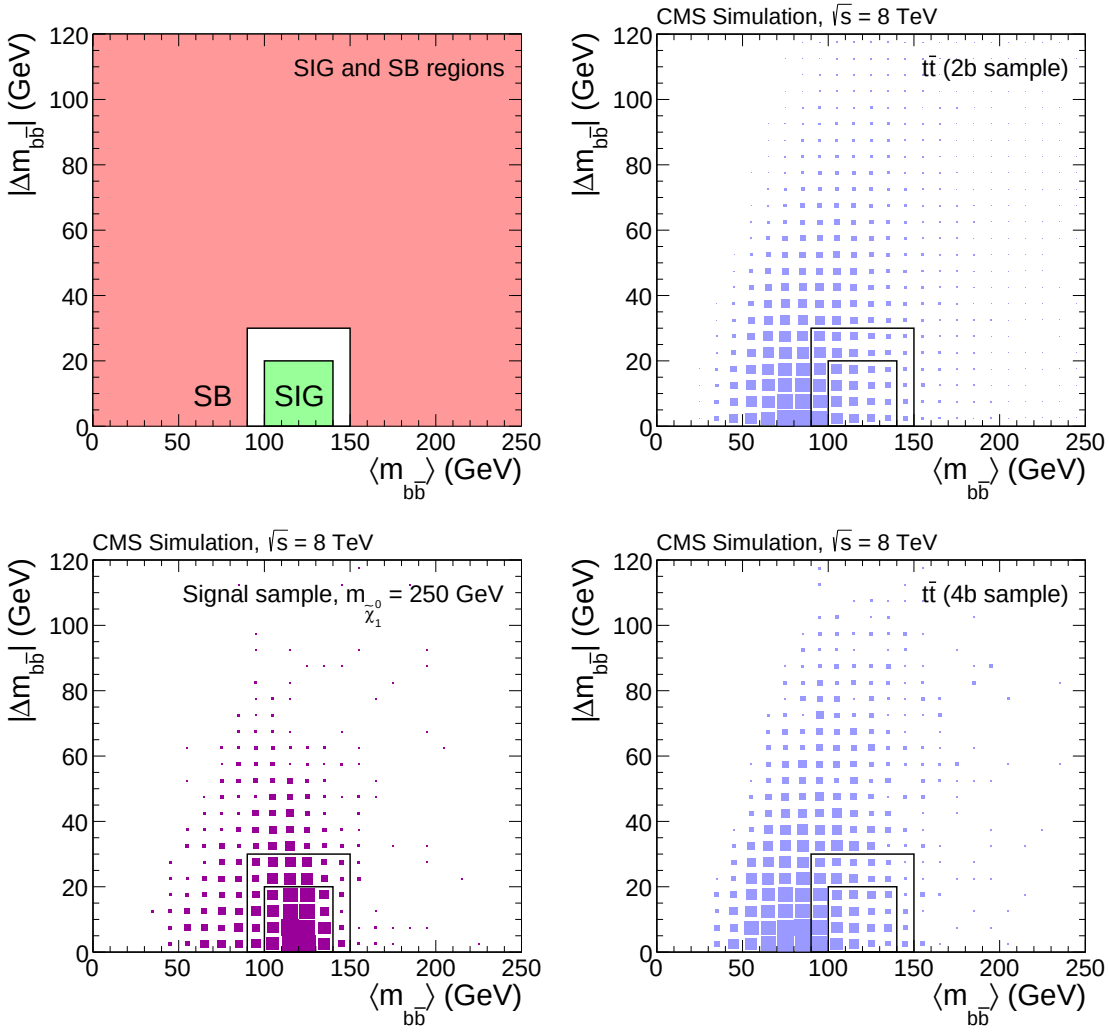

Figure 3: (top left) Illustration of the signal (SIG) and sideband (SB) regions in the $|\Delta m_{\mathrm{b\bar{b}}}|$ versus $\langle m_{\mathrm{b\bar{b}}} \rangle$ plane of the hh $\to$ b$\bar{\mathrm{b}}$b$\bar{\mathrm{b}}$ analysis; (top right and bottom right) Distributions of simulated t$\bar{\mathrm{t}}$ events in the 2b and 4b samples; (bottom left) Distribution of simulated signal events in the 4b sample for a $\tilde{\chi}_1^0$ higgsino mass value of 250 GeV and an LSP (gravitino) mass of 1 GeV. The plots employ an arbitrary integrated luminosity.

dominant background, from the class of t$\bar{\mathrm{t}}$ events described above, three jets tend to lie in the same hemisphere while the fourth jet lies in the opposite hemisphere, making ΔR_{max} relatively large.

A signal region (SIG) is defined using the variables $|\Delta m_{\mathrm{b\bar{b}}}|$, ΔR_{max}, and the average of the two Higgs boson candidate mass values $\langle m_{\mathrm{b\bar{b}}} \rangle \equiv (m_{\mathrm{b\bar{b}},1} + m_{\mathrm{b\bar{b}},2})/2$. We require

- $|\Delta m_{\mathrm{b\bar{b}}}| < 20\,\mathrm{GeV}$;
- $\Delta R_{\mathrm{max}} < 2.2$;
- $100 < \langle m_{\mathrm{b\bar{b}}} \rangle < 140\,\mathrm{GeV}$.

These requirements are determined through an optimization procedure that takes into consideration both the higgsino discovery potential and the ability to set stringent limits in the case of non-observation. Distributions of these variables for events in the 4b event sample are shown in Fig. 2.

Table 1: Observed numbers of events and corresponding SM background estimates in bins of E_T^{miss}-significance $\mathcal{S}_{MET}$ for the $hh \to b\bar{b}b\bar{b}$ analysis. For the SM background estimate, the first uncertainty is statistical and the second systematic. Numerical results for example signal scenarios are given in Tables 8 and 9 of Appendix B.

$\mathcal{S}_{MET}$ bin	$\mathcal{S}_{MET}$ range	SM background (3b-SIG)	Data (3b-SIG)	SM background (4b-SIG)	Data (4b-SIG)
1	$30-50$	$6.7^{+1.4+1.0}_{-1.1-0.7}$	4	$2.9^{+0.8+0.5}_{-0.6-0.4}$	4
2	$50-100$	$11.6^{+1.9+0.9}_{-1.6-0.7}$	15	$4.9^{+1.1+1.4}_{-0.9-0.9}$	7
3	$100-150$	$2.44^{+0.84+0.56}_{-0.64-0.35}$	1	$0.59^{+0.39+0.09}_{-0.26-0.09}$	3
4	>150	$1.50^{+0.82+0.64}_{-0.54-0.32}$	0	$0.40^{+0.39+0.26}_{-0.22-0.10}$	0

A sideband region (SB) is defined by applying the SIG-region criteria except using the area outside the following rectangle in the $|\Delta m_{b\bar{b}}|$-$\langle m_{b\bar{b}} \rangle$ plane:

- $|\Delta m_{b\bar{b}}| < 30\,\text{GeV}$;
- $90 < \langle m_{b\bar{b}} \rangle < 150\,\text{GeV}$.

Schematic representations of the SIG and SB regions are shown in Fig. 3 (upper left).

To illustrate the basic principle of our background determination method, consider the 4b and 2b samples. We can define four observables, denoted A, B, C, and D:

- A: number of background events in the 4b-SIG region;
- B: number of background events in the 4b-SB region;
- C: number of background events in the 2b-SIG region;
- D: number of background events in the 2b-SB region.

We assume that the ratio of the number of background events in the SIG region to that in the SB region, denoted the SIG/SB ratio, is the same for the 2b and 4b samples. This assumption is supported by (for example) the similarity between the 2b and 4b results shown in the top-right and bottom-right plots of Fig. 3. We further assume that the 2b-SIG and all SB regions are dominated by background. The prediction for the number of background events in the 4b-SIG region is then given by the algebraic expression $A = (C/D)\,B$. The same result applies replacing the 4b sample by the 3b sample in the above discussion.

In practice, we examine the data in four bins of $\mathcal{S}_{MET}$, which are indicated in Table 1. The numbers of background events in the four $\mathcal{S}_{MET}$ bins of the 2b-SIG, 3b-SIG, and 4b-SIG regions are determined simultaneously in a likelihood fit, with the SIG/SB ratios for background in all three b-jet samples constrained to a common value (determined in the fit) for each $\mathcal{S}_{MET}$ bin separately. Figure 4 shows the predictions of the SM simulation for the SIG/SB ratios, in the four bins of $\mathcal{S}_{MET}$, for the three b-jet samples (for purposes of comparison, the data are also shown). It is seen that the SIG/SB ratio of SM events for $\mathcal{S}_{MET}$ bin 1 is predicted to be about the same for all three b-jet samples, and similarly for the other three $\mathcal{S}_{MET}$ bins, supporting the key assumption of the method. Figure 4 includes the results determined from the likelihood fit for the SIG/SB ratio in each bin, assuming the SUSY signal yield to be zero.

To evaluate the systematic uncertainty of the background estimate, we consider two terms, determined from simulation, which are treated as separate nuisance parameters in the likelihood fit. The first term, determined for each bin of $\mathcal{S}_{MET}$ in the 4b (3b) sample, is given by the larger

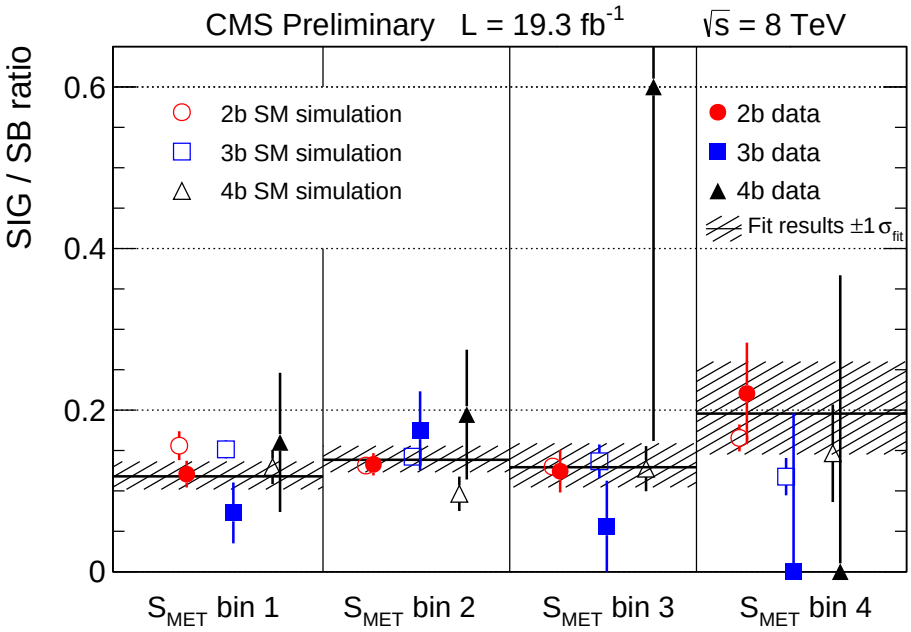

Figure 4: The ratio of the number of events in the signal (SIG) region to that in the sideband (SB) region as a function of $\mathcal{S}_{\mathrm{MET}}$ bin (see Table 1), for the 2b, 3b, and 4b event samples of the $\mathrm{hh} \to \mathrm{b\bar{b}b\bar{b}}$ analysis. The simulated results account for the various expected SM processes. The results of a likelihood fit to data, in which the SIG/SB ratio is determined separately for each bin, is also shown.

of the difference from unity of the double ratio R, with R the SIG/SB ratio of 4b (3b) events divided by the SIG/SB ratio of 2b events ("non-closure result"), or the statistical uncertainty of R. The size of this uncertainty varies between around 14 and 40%, with a typical value of 25%. The second term accounts for potential differences between the SIG/SB ratio of $\mathrm{t\bar{t}}$ and QCD multijet events as well as for the possibility that the relative fraction of $\mathrm{t\bar{t}}$ and QCD multijet events varies between the 2b, 3b, and 4b samples or bins of $\mathcal{S}_{\mathrm{MET}}$. From simulation, the relative fraction of background events due to QCD multijet events varies by 6% (between 1 and 7%), depending primarily on the bin of $\mathcal{S}_{\mathrm{MET}}$. We conservatively allow up to a 20% variation in this fraction and determine a corresponding 7% increase in the non-closure result, which we define as the associated uncertainty.

The observed numbers of events in the 3b-SIG and 4b-SIG regions are shown in Fig. 5 as a function of $\mathcal{S}_{\mathrm{MET}}$, in comparison with the SM background predictions from the likelihood fit and the predictions of two signal scenarios. Numerical values are given in Table 1.

6 Search in the hh, hZ, and hW channels with one $\mathrm{h} \to \gamma\gamma$ decay

We next describe our searches for hh, hZ, and hW states in channels with one Higgs boson that decays to photons. While the $\mathrm{h} \to \gamma\gamma$ branching fraction is small [68], the expected diphoton invariant-mass signal peak is narrow, allowing the SM background to be reduced. For the hh combination, we search in channels in which the second Higgs boson decays according to $\mathrm{h} \to \mathrm{b\bar{b}}$, WW, ZZ, or $\tau\tau$, where, in the case of these last three modes, at least one electron or muon is required to be present in the final state. For the hZ and hW combinations, we search in the channels in which the Z or W boson either decays to two light-flavor jets or leptonically, where the leptonic decays yield at least one electron or muon.

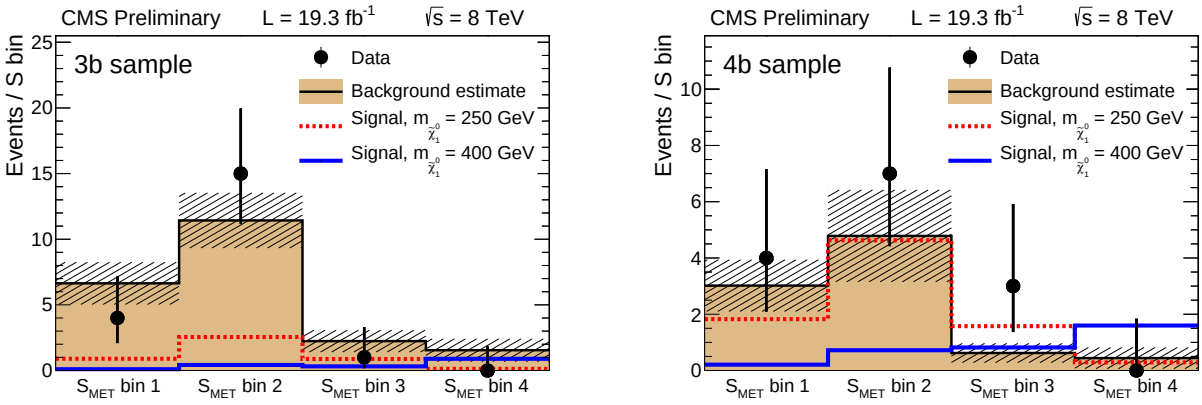

Figure 5: Observed numbers of events as a function of $E_{\mathrm{T}}^{\mathrm{miss}}$ significance ($\mathcal{S}_{\mathrm{MET}}$) bin for the $\mathrm{hh} \to \mathrm{b\bar{b}b\bar{b}}$ analysis, in comparison with the SM background estimate from the likelihood fit, for the (left) 3b-SIG and (right) 4b-SIG regions. The hatched bands show the total uncertainty of the background prediction, with statistical and systematic terms combined. The expected (unstacked) results for signal events, with $\widetilde{\chi}_1^0$ higgsino mass values of 250 and 400 GeV and an LSP (gravitino) mass of 1 GeV, are also shown.

Photon candidates are reconstructed from "superclusters" of energy deposited in the electromagnetic calorimeter [69, 70], with energies determined using multivariate regression [24, 70]. To reduce contamination from electrons misidentified as photons, photon candidates are rejected if they register hit patterns in the pixel detector that are consistent with a track. The photon candidates are required to satisfy loose identification criteria based primarily on their shower shape and isolation [71]. Signal events tend to produce decay products in the central region of the detector, because of the large masses of the produced SUSY particles. Therefore, photon candidates are restricted to $|\eta| < 1.44$.

Events must contain at least one photon candidate with $p_{\mathrm{T}} > 40\,\mathrm{GeV}$ and another with $p_{\mathrm{T}} > 25\,\mathrm{GeV}$. The $\mathrm{h} \to \gamma\gamma$ boson candidate is formed from the two highest-p_{T} photons in the event. The resulting diphoton invariant mass $m_{\gamma\gamma}$ is required to appear in the Higgs boson mass region defined by $120 < m_{\gamma\gamma} < 131\,\mathrm{GeV}$.

For the searches described in this section, jets must have $p_{\mathrm{T}} > 30\,\mathrm{GeV}$ and $|\eta| < 2.4$. Tagged b jets are defined using the CSV-medium criteria.

6.1 $\mathrm{hh} \to \gamma\gamma\mathrm{b\bar{b}}$

For the search in the $\mathrm{h}(\to \gamma\gamma)\mathrm{h}(\to \mathrm{b\bar{b}})$ channel, we require

- exactly two tagged b jets, which together form the $\mathrm{h} \to \mathrm{b\bar{b}}$ candidate;
- the invariant mass $m_{\mathrm{b\bar{b}}}$ of the two tagged b jets to lie in the Higgs boson mass region defined by $95 < m_{\mathrm{b\bar{b}}} < 155\,\mathrm{GeV}$;
- no identified, isolated electron or muon candidate, where the lepton identification criteria require $p_{\mathrm{T}} > 15\,\mathrm{GeV}$ and $|\eta| < 2.4$, with isolation requirements $R_{\mathrm{iso}} < 0.15$ for electrons and $R_{\mathrm{iso}} < 0.12$ for muons.

The distribution of $m_{\gamma\gamma}$ for the selected events is shown in Fig. 6. The principal background arises from events in which a neutral hadron is misidentified as a photon.

The SM background, with the exception of the generally small contribution from SM Higgs boson production, is evaluated using $m_{\gamma\gamma}$ data sidebands defined by $103 \leq m_{\gamma\gamma} \leq 118\,\mathrm{GeV}$

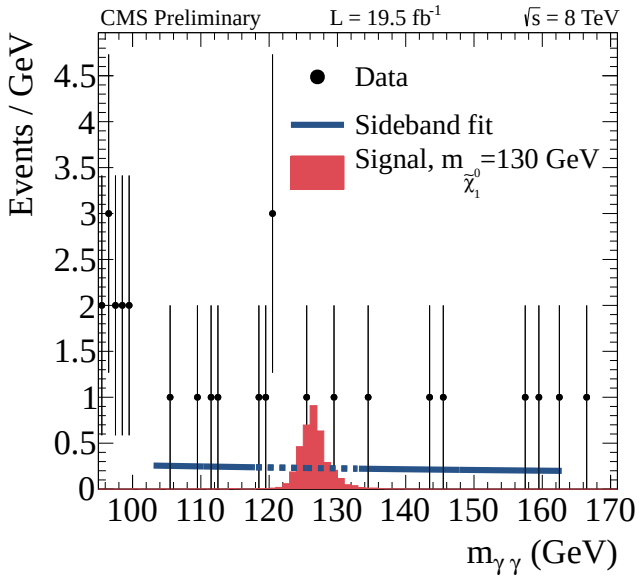

Figure 6: Distribution of diphoton invariant mass $m_{\gamma\gamma}$ after all selection criteria are applied except for that on $m_{\gamma\gamma}$, for the $\mathrm{h}(\to \gamma\gamma)\mathrm{h}(\to \mathrm{b\bar{b}})$ search. The result of a fit to a power-law function using data in the sideband regions (see text) is indicated by the solid line. The dotted line shows an interpolation of the fitted function into the Higgs boson mass region excluded from the fit. The expected results for signal events, with a $\tilde{\chi}_1^0$ higgsino mass value of 130 GeV and an LSP (gravitino) mass of 1 GeV, are also shown.

Table 2: Observed numbers of events and corresponding SM background estimates, in bins of Higgs-boson-candidate variable $S_{\mathrm{T}}^{\mathrm{h}}$ (see text), for the $\mathrm{hh} \to \gamma\gamma\mathrm{b\bar{b}}$ analysis. The uncertainties shown for the SM background estimates are the combined statistical and systematic terms, while those shown for signal events are statistical. The expected yields for signal events, with a higgsino mass value of 130 GeV and an LSP (gravitino) mass of 1 GeV, are also shown.

$S_{\mathrm{T}}^{\mathrm{h}}$ bin (GeV)	SM background	Data	hh events, $m_{\tilde{\chi}_1^0} = 130$ GeV
0-60	$0.21^{+0.28}_{-0.21}$	1	0.28 ± 0.03
60-120	$0.95^{+0.99}_{-0.95}$	2	0.63 ± 0.04
120-180	$0.21^{+0.29}_{-0.21}$	1	0.55 ± 0.04
180-240	0.74 ± 0.38	0	0.53 ± 0.04
> 300	$0.42^{+0.49}_{-0.42}$	1	1.46 ± 0.06

and $133 \leq m_{\gamma\gamma} \leq 163$ GeV. We construct the quantity $S_{\mathrm{T}}^{\mathrm{h}}$, which is the scalar sum of the p_{T} values of the two Higgs boson candidates. The distribution of $S_{\mathrm{T}}^{\mathrm{h}}$ is measured separately in each of the two sidebands. Each sideband distribution is then normalized to correspond to the expected number of background events in the signal region. To determine the expected number of background events in the signal region, we perform a likelihood fit of a power-law function to the $m_{\gamma\gamma}$ distribution between 103 and 163 GeV, excluding the $118 < m_{\gamma\gamma} < 133$ GeV region around the Higgs boson mass. The result of this fit is shown by the solid (blue) curve in Fig. 6. The scaled distributions of $S_{\mathrm{T}}^{\mathrm{h}}$ from the two sidebands are found to be consistent with each other and are averaged. This average is taken to be the estimate of the SM background (other than from SM Higgs production), with half the difference assigned as a systematic uncertainty.

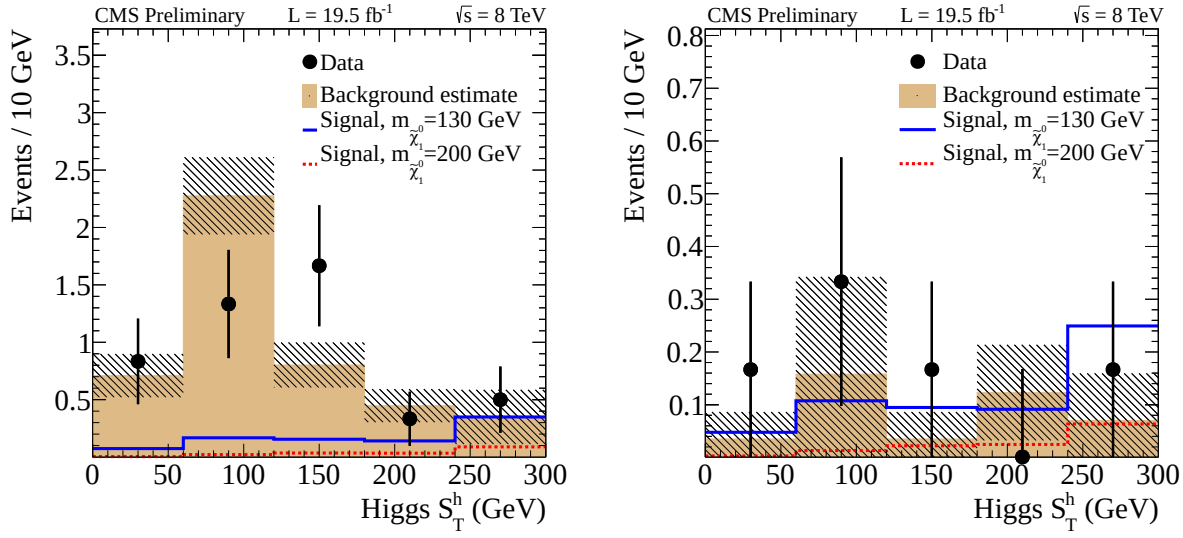

Figure 7: Observed numbers of events as a function of the scalar sum of p_T values of the two Higgs boson candidates, S_T^h, for the hh → γγbb̄ analysis, in comparison with the SM background estimate, (left) for a control sample with loose tagging requirements for b jets, and (right) for the nominal selection. The hatched bands show the total uncertainty of the background prediction, with statistical and systematic terms combined. The (unstacked) results for signal events, with $\tilde{\chi}_1^0$ higgsino mass values of 130 and 200 GeV and an LSP (gravitino) mass of 1 GeV, are also shown.

To account for the background from SM Higgs boson production, which peaks in the $m_{\gamma\gamma}$ signal region and is not accounted for with the above procedure, we use simulated events. A systematic uncertainty of 30% is assigned to this result, which accounts both for the uncertainty of the SM Higgs boson cross section [68] and for potential misrepresentation of the data by the simulation in the tails of kinematic variables like S_T^h.

Fig. 7 (left) shows the distribution of S_T^h for a sample of events selected in the same manner as the nominal sample except, for improved statistical precision, with loose CSV requirements for b-jet tagging. The distributions for two signal scenarios, and for the SM background determined as described above, are also shown. It is seen that S_T^h tends to be larger in signal events than in background events, providing discrimination between the two.

The corresponding results for the nominal selection criteria are shown in Fig. 7 (right), with numerical values in Table 2.

6.2 hZ and hW → γγ+2 jets

For hZ and hW combinations with h → γγ and either W → 2 jets or Z → 2 jets, the vector boson candidate is formed from two jets that yield a dijet mass m_{jj} consistent with the mass of a W or Z boson, $70 < m_{jj} < 110$ GeV. Multiple candidates per event are allowed. The fraction of events with multiple candidates is 16%. The average number of candidates per event is 1.2. Events with isolated electrons or muons are rejected, using the criteria of Section 6.1. To avoid overlap with the sample discussed in Section 6.1, events are rejected if a loose-tagged b jet combined with a medium-tagged b jet yields an invariant mass in the range $95 < m_{b\bar{b}} < 155$ GeV. The distribution of $m_{\gamma\gamma}$ for the selected events is shown in Fig. 8 (left).

The SM background estimate is obtained using the procedure described in Section 6.1 except

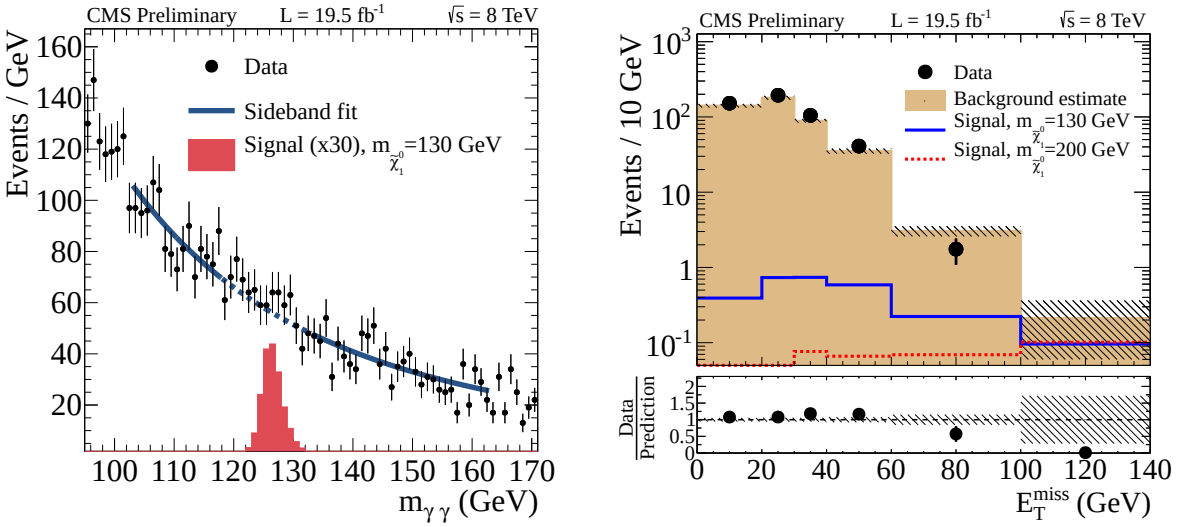

Figure 8: Results for the hZ and hW → γγ+2 jets analysis after all selection criteria are applied except for that on the displayed variable. (left) Distribution of diphoton invariant mass $m_{\gamma\gamma}$. The result of a fit to a power-law function using data in the sideband regions (see text) is indicated by the solid line. The dotted line shows an interpolation of the fitted function into the Higgs boson mass region excluded from the fit. The expected result for hZ signal events with a $\widetilde{\chi}_1^0$ higgsino mass of 130 GeV and an LSP (gravitino) mass of 1 GeV, multiplied by a factor of 30 for better visibility, is also shown. (right) Observed numbers of events as a function of $E_{\mathrm{T}}^{\mathrm{miss}}$ in comparison with the SM background estimate. The hatched bands show the total uncertainty of the background prediction, with statistical and systematic terms combined. The expected (unstacked) results for hZ signal events, with the indicated values of the $\widetilde{\chi}_1^0$ higgsino mass and an LSP (gravitino) mass of 1 GeV, are also shown.

using the $E_{\mathrm{T}}^{\mathrm{miss}}$ variable rather than the $S_{\mathrm{T}}^{\mathrm{h}}$ variable, viz., from the average of the scaled $E_{\mathrm{T}}^{\mathrm{miss}}$ distributions derived from the two $m_{\gamma\gamma}$ sidebands, summed with the prediction from simulated SM Higgs boson events. The solid (blue) curve in Fig. 8 (left) shows the result of the power-law fit to the $m_{\gamma\gamma}$ sideband regions. The scaled $E_{\mathrm{T}}^{\mathrm{miss}}$ distributions from the two sidebands are found to be consistent with each other within their uncertainties.

The measured distribution of $E_{\mathrm{T}}^{\mathrm{miss}}$ for the selected events is shown in Fig. 8 (right) in comparison with the SM background estimate and with the predictions from two signal scenarios. Numerical values are given in Table 3.

6.3 hh, hZ, and hW → γγ+leptons

We next consider hh, hZ, and hW combinations in which a Higgs boson decays according to h → γγ while the other boson (h, Z, or W) decays to a final state with at least one lepton (electron or muon). For the hh channel this signature encompasses events in which the second Higgs boson decays according to h → ZZ, WW, or ττ, followed by the leptonic decay of at least one Z, W, or τ particle, including situations where one Z boson decays to charged leptons and the other to neutrinos.

The lepton identification criteria are the same as those presented in Section 6.1 with the additional requirement that the ΔR separation between an electron or muon candidate and each of the two photon candidates exceed 0.3. To reduce background in which an electron is misidentified as a photon, events are eliminated if the invariant mass formed between an electron

Table 3: Observed numbers of events and corresponding SM background estimates, in bins of missing transverse energy E_T^{miss}, for the hV → γγ+2 jets analysis, where V represents a W or Z boson. The uncertainties shown for the SM background estimates are the combined statistical and systematic terms, while those shown for signal events are statistical. The expected yields for hZ signal events, with a higgsino mass value of 130 GeV and an LSP (gravitino) mass of 1 GeV, are also shown.

E_T^{miss} (GeV)	SM background	Data	hZ events, $m_{\tilde{\chi}_1^0}$ = 130 GeV
0-20	288 ± 15	305	0.76 ± 0.03
20-30	183 ± 10	195	0.71 ± 0.03
30-40	91.1 ± 4.7	105	0.72 ± 0.03
40-60	72.0 ± 5.0	82	1.14 ± 0.04
60-100	12.5 ± 1.9	7	0.87 ± 0.03
>100	0.96 ± 0.61	0	0.37 ± 0.02

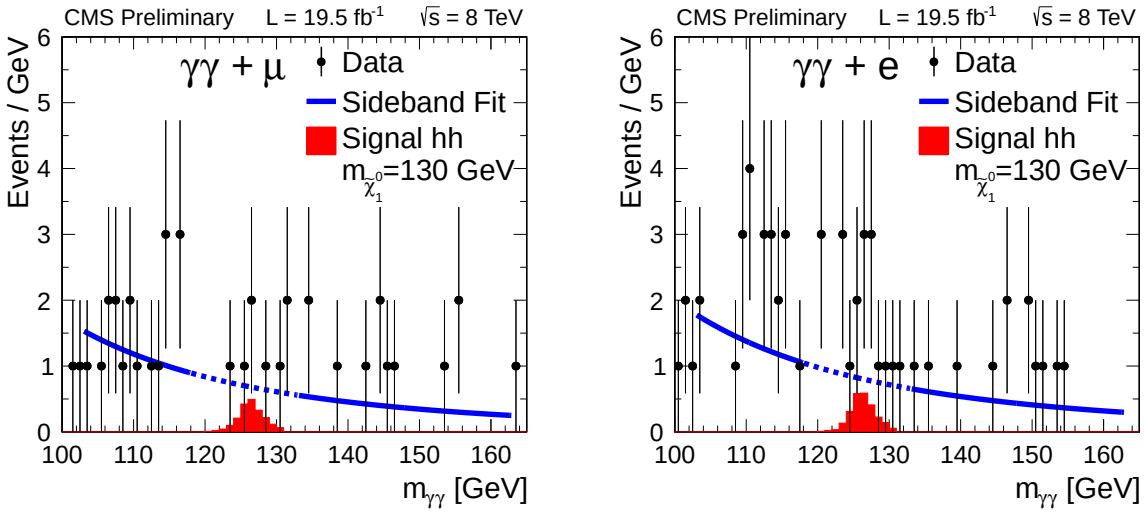

Figure 9: The distribution of diphoton invariant mass $m_{\gamma\gamma}$ after all selection criteria are applied except for that on $m_{\gamma\gamma}$, for the hh, hZ, and hW → γγ+leptons analysis, for the (left) muon and (right) electron samples. The result of a fit to a power-law function using data in the sideband regions (see text) is indicated by the solid line. The dotted line shows an interpolation of the fitted function into the Higgs boson mass region excluded from the fit. The expected results for hh events, with a $\tilde{\chi}_1^0$ higgsino mass value of 130 GeV and an LSP (gravitino) mass of 1 GeV, are also shown.

candidate and one of the two h → γγ photon candidates lies in the Z boson mass region $86 < m_{e\gamma} < 96$ GeV. Electron candidates are rejected if they appear within $1.44 < |\eta| < 1.57$, which represents a transition region between the barrel and endcap electromagnetic calorimeters [39] where the reconstruction efficiency is difficult to model. To prevent overlap with the other searches, events are allowed to contain at most one medium-tagged b jet.

We select a sample with at least one muon and an orthogonal sample with no muons but at least one electron. We refer to these samples as the muon and electron samples, respectively. About 93% of the events in each sample contain a single electron or muon, and there are no events for which the sum of electron and muon candidates exceeds two (only two events have one electron and one muon). The $m_{\gamma\gamma}$ distributions for the two samples are shown in Fig. 9.

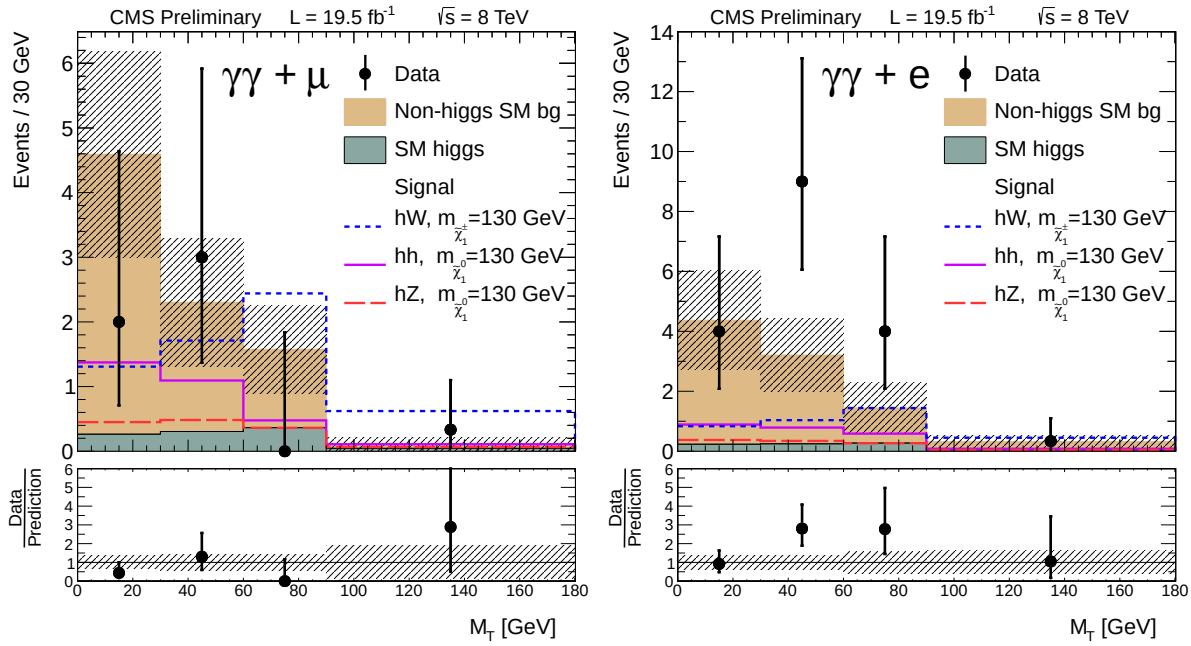

Figure 10: Observed numbers of events as a function of transverse mass M_{T} for the hh, hZ, and hW $\to \gamma\gamma$+leptons analysis, in comparison with the (stacked) SM background estimates, for the (left) muon and (right) electron samples. The hatched bands show the total uncertainty of the background prediction, with statistical and systematic terms combined. The (unstacked) results for various signal scenarios are also shown. For the hh and hZ scenarios, the higgsino mass is 130 GeV and the LSP (gravitino) mass is 1 GeV. For the hW scenario, $\mathrm{m}_{\widetilde{\chi}_2^0} = \mathrm{m}_{\widetilde{\chi}_1^\pm} = 130$ GeV and $m_{\widetilde{\chi}_1^0} = 1$ GeV [see Fig. 1 (right)].

The SM background is evaluated in the same manner as described in Section 6.1 except using the transverse mass variable $M_{\mathrm{T}} \equiv \sqrt{2E_{\mathrm{T}}^{\mathrm{miss}} p_{\mathrm{T}}^{\ell}[1-\cos(\Delta\phi_{\ell,E_{\mathrm{T}}^{\mathrm{miss}}})]}$ in place of the $S_{\mathrm{T}}^{\mathrm{h}}$ variable, where p_{T}^{ℓ} is the transverse momentum of the highest p_{T} lepton, with $\Delta\phi_{\ell,E_{\mathrm{T}}^{\mathrm{miss}}}$ the difference in azimuthal angle between the p_{T}^{ℓ} and $E_{\mathrm{T}}^{\mathrm{miss}}$ vectors. For SM background events with W bosons, the M_{T} distribution exhibits an endpoint near the W boson mass. In contrast, for signal events, the value of M_{T} can be much larger. As an alternative, we tested use of the $E_{\mathrm{T}}^{\mathrm{miss}}$ distribution to evaluate the SM background and found the M_{T} distribution to be slightly more sensitive.

The SM background estimate is thus given by the average of the scaled M_{T} distributions from the two $m_{\gamma\gamma}$ sidebands, summed with with the contribution from simulated SM Higgs boson events. The solid (blue) curves in Fig. 9 show the results of the power-law fits to the $m_{\gamma\gamma}$ sideband regions. For the electron channel [Fig. 9 (right)], a cluster of events is visible at $m_{\gamma\gamma} \approx 112$ GeV. We verified that the prediction for the number of SM events in the signal region $120 < m_{\gamma\gamma} < 131$ GeV is stable to within about one standard deviation of the statistical uncertainty for alternative definitions of the sidebands, viz. $110 < m_{\gamma\gamma} < 118$ GeV for the lower sideband.

The M_{T} distributions of the selected events are presented in Fig. 10. Numerical values are given in Table 4. The background estimates and predictions from several signal scenarios are also shown. Results for the alternative method to evaluate the SM background, based on the $E_{\mathrm{T}}^{\mathrm{miss}}$ distribution rather than the M_{T} distribution, are shown in Fig. 19 of Appendix A.

Table 4: Observed numbers of events and corresponding SM background estimates, in bins of transverse mass M_T, for the hh, hZ, and hW $\to \gamma\gamma$+leptons analysis. The uncertainties shown for the SM background estimates are the combined statistical and systematic terms, while those shown for signal events are statistical. The column labeled "hW events" shows the expected number of events from the chargino-neutralino pair-production process of Fig. 1 (right), taking $m_{\tilde{\chi}_2^0} = m_{\tilde{\chi}_1^\pm} = 130\,\text{GeV}$ and $m_{\tilde{\chi}_1^0} = 1\,\text{GeV}$.

	Muon sample			Electron sample		
M_T (GeV)	SM Background	Data	hW events	SM background	Data	hW events
$0-30$	4.6 ± 1.6	2	1.2 ± 0.1	4.4 ± 1.7	4	0.80 ± 0.06
$30-60$	2.31 ± 0.99	3	1.6 ± 0.1	3.2 ± 1.2	9	1.0 ± 0.1
$60-90$	1.59 ± 0.68	0	2.3 ± 0.1	1.44 ± 0.85	4	1.5 ± 0.1
>90	0.35 ± 0.30	1	1.7 ± 0.1	0.96 ± 0.58	1	1.4 ± 0.1

7 Search in the hZ channel with $h \to b\bar{b}$ and $Z \to \ell^+\ell^-$

We now describe our search in the SUSY hZ channel with $h \to b\bar{b}$ and $Z \to \ell^+\ell^-$ (ℓ = e, μ). Electron and muon candidates are required to satisfy $p_T > 20\,\text{GeV}$, $|\eta| < 2.4$, and $R_{iso} < 0.15$. For the R_{iso} variable, a cone size $R_{cone} = 0.3$ is used for both electrons and muons, rather than $R_{cone} = 0.4$ for muons as in Sections 5 and 6. Electron candidates that appear within the transition region $1.44 < |\eta| < 1.57$ between the barrel and endcap electromagnetic calorimeters are rejected. Jets must satisfy $p_T > 30\,\text{GeV}$ and $|\eta| < 2.5$ and be separated by more than $\Delta R = 0.4$ from an electron or muon candidate. To be tagged as a b jet, the jet must satisfy the CSV-medium criteria.

Events are required to contain

- exactly one e^+e^- or $\mu^+\mu^-$ pair with a dilepton invariant mass $m_{\ell\ell}$ in the Z boson mass region $81 < m_{\ell\ell} < 101\,\text{GeV}$;
- no third electron or muon candidate, selected using the above criteria except with $p_T > 10\,\text{GeV}$;
- no hadronically decaying τ lepton candidate with $p_T > 20\,\text{GeV}$;
- at least two tagged b jets, where the two most b-like jets yield a dijet mass in the Higgs boson mass region $100 < m_{b\bar{b}} < 150\,\text{GeV}$.

The reason to reject events with a third lepton is to avoid overlap with the three-or-more lepton sample discussed in Section 8.

Events with a $t\bar{t}$ pair represent a large potential source of background, especially if both top quarks decay to a state with a lepton. To reduce this background, we use the M_{T2}^j variable [72, 73], which corresponds to the minimum mass of a pair-produced parent particle compatible with the observed four-momenta in the event, where each parent is assumed to decay to a b jet, a charged lepton, and an undetected particle, and where the vector sum of the p_T values of the two undetected particles is assumed to equal the observed result for E_T^{miss}. For $t\bar{t}$ events with perfect event reconstruction, M_{T2}^j has an upper bound at the top-quark mass. For signal events, M_{T2}^j can be much larger. To account for imperfect reconstruction and finite detector resolution, we require $M_{T2}^j > 200\,\text{GeV}$.

We further require $E_T^{miss} > 60$, 80, or 100 GeV, where the lower bound on E_T^{miss} depends on

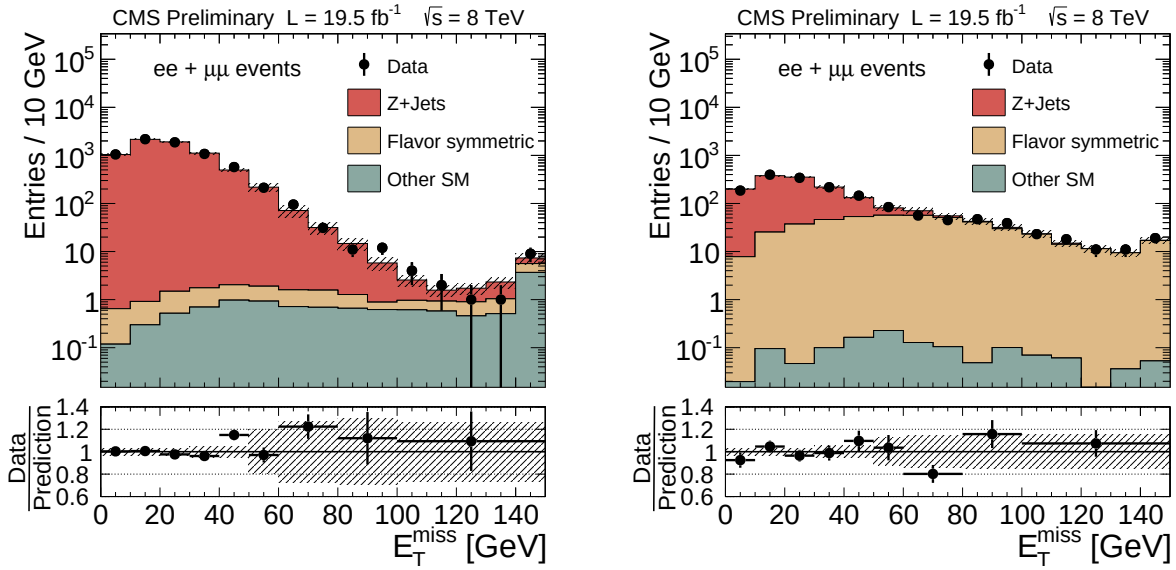

Figure 11: The distribution of $E_{\mathrm{T}}^{\mathrm{miss}}$ in comparison with the (stacked) SM background estimates for the $\mathrm{h}(\rightarrow \mathrm{b\bar{b}})\mathrm{Z}(\rightarrow \ell^{+}\ell^{-})$ analysis, for data control samples enriched in (left) SM Z+jets events, and (right) $\mathrm{t\bar{t}}$ events. The hatched bands in the ratio plots (lower panels) indicate the uncertainty of the total background prediction, with statistical and systematic terms combined.

which choice yields the largest expected signal sensitivity for a given value of the higgsino mass.

The remaining background mostly consists of events from SM Z+jets, $\mathrm{t\bar{t}}$, $\mathrm{W^{+}W^{-}}$, $\tau^{+}\tau^{-}$, and tW single-top-quark production. These backgrounds are evaluated using data, as described below. Other remaining SM background processes are combined into an "other" category, which is evaluated using simulation and assigned an uncertainty of 50%. The "other" category includes background from ZW and ZZ boson pair production, $\mathrm{t\bar{t}}$ processes with an associated W or Z boson, and processes with three vector bosons.

For the SM Z+jets background, significant values of $E_{\mathrm{T}}^{\mathrm{miss}}$ arise primarily because of the mismeasurement of jet p_{T}. Another source is the semileptonic decay of charm and bottom quarks. As in Ref. [74], we evaluate this background using a sample of γ+jets events, which is selected using similar criteria to those used for the nominal selection, including the same b-jet tagging requirements and restriction on $m_{\mathrm{b\bar{b}}}$. We account for kinematic differences between the γ+jets and signal samples by reweighting the H_{T} and boson-p_{T} spectra of the former sample to match those of the latter, where H_{T} is the scalar sum of jet p_{T} values. The resulting γ+jets $E_{\mathrm{T}}^{\mathrm{miss}}$ distributions are then normalized to unit area to define templates. Two different templates are formed: one from γ+jets events with exactly two jets, and one from the events with three or more jets. The SM Z+jets background estimate is given by the sum of the two templates, each weighted by the number of events in the signal sample with the respective jet multiplicity. To account for the small level of background expected in the signal sample from SM processes other than SM Z+jets production, which is mostly due to $\mathrm{t\bar{t}}$ production, the prediction is normalized to the data yield in the $0 < E_{\mathrm{T}}^{\mathrm{miss}} < 50\,\mathrm{GeV}$ region, where the contribution of SM Z+jets events dominates. The impact of signal events on the estimate of the SM Z+jets background is found to be negligible. The corresponding systematic uncertainty is evaluated by varying the criteria used to select γ+jets events, by assessing the impact of $\mathrm{t\bar{t}}$ events, and by determining the difference between the predicted and genuine SM Z+jets event yields when the simulation is used to describe the γ+jets and signal samples. The three sources of systematic uncertainty

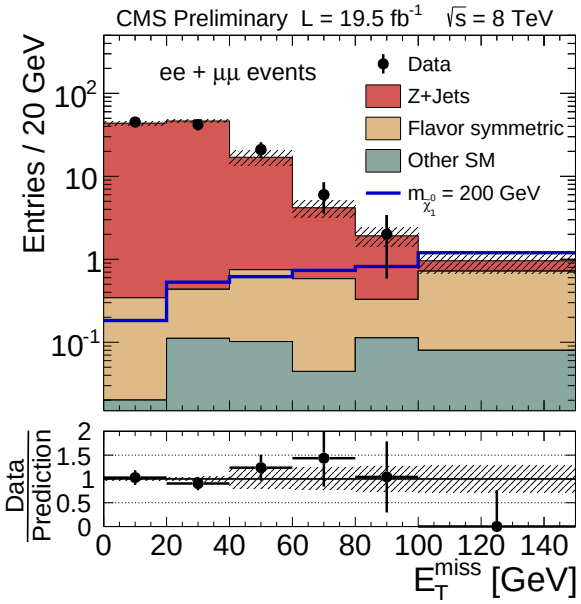

Figure 12: Observed numbers of events as a function of E_T^{miss} for the $h(\to b\bar{b})Z(\to \ell^+\ell^-)$ analysis, in comparison with the (stacked) SM background estimates. The (unstacked) results for a $\tilde{\chi}_1^0$ higgsino mass of 200 GeV and an LSP (gravitino) mass of 1 GeV are also shown. The hatched band in the ratio plot (lower panel) indicates the uncertainty of the total background prediction, with statistical and systematic terms combined.

are added in quadrature to define the total systematic uncertainty.

For the $t\bar{t}$, W^+W^-, $\tau^+\tau^-$, and tW background, the rate of decay to events with exactly one electron and exactly one muon is the same as the rate of decay to events with either exactly one e^+e^- or one $\mu^+\mu^-$ pair, once the difference between the electron and muon reconstruction efficiencies is taken into account. We therefore refer to this category of events as the "flavor symmetric" (FS) background. The FS background is evaluated using a sample of $e\mu$ events selected in the manner described above for the e^+e^- and $\mu^+\mu^-$ samples except without the requirement on the dilepton mass: instead of applying an invariant mass restriction $81 < m_{e\mu} < 101$ GeV in analogy with the mass restriction imposed on $m_{\ell\ell}$, we apply a factor, derived from simulation, that gives the probability for $m_{e\mu}$ to fall into this interval, with a systematic uncertainty defined by the difference between this factor in data and simulation. This procedure yields improved statistical precision compared to the result based on an $m_{e\mu}$ requirement [74].

The background evaluation procedures are validated using data control samples enriched in the principal background components. As an example, Fig. 11 (left) shows the E_T^{miss} distribution for a control sample selected in the same manner as the standard sample except with the requirement that there be no tagged b jet: this yields a sample dominated by SM Z+jets events. Fig. 11 (right) show the results for a sample selected with the nominal requirements except with the M_{T2}^j requirement inverted: this yields a sample dominated by $t\bar{t}$ events. For both these control samples, the SM background estimate is seen to accurately represent the data.

The distribution of E_T^{miss} for the selected events is presented in Fig. 12 in comparison with the corresponding background prediction and with the prediction from a signal scenario. Numerical values are given in Table 5.

Table 5: Observed numbers of events and corresponding SM background estimates, in bins of missing transverse energy $E_{\mathrm{T}}^{\mathrm{miss}}$, for the $\mathrm{h}(\to \mathrm{b\bar{b}})\mathrm{Z}(\to \ell^+\ell^-)$ analysis. The uncertainties shown for the SM background estimates are the combined statistical and systematic terms, while those shown for signal events are statistical. For bins with $E_{\mathrm{T}}^{\mathrm{miss}} > 60\,\mathrm{GeV}$, signal event yields are given for four values of the $\widetilde{\chi}_1^0$ higgsino mass, with an LSP (gravitino) mass of 1 GeV.

	$E_{\mathrm{T}}^{\mathrm{miss}} < 25\,\mathrm{GeV}$	$25 < E_{\mathrm{T}}^{\mathrm{miss}} < 50\,\mathrm{GeV}$	$50 < E_{\mathrm{T}}^{\mathrm{miss}} < 60\,\mathrm{GeV}$
Z+jets bkg	56.7 ± 1.9	43.3 ± 2.3	5.7 ± 1.2
Flavor symmetric	0.4 ± 0.3	0.4 ± 0.3	0.4 ± 0.3
Other SM bkg	< 0.1	0.1 ± 0.1	0.1 ± 0.1
Total SM bkg	57.2 ± 1.9	43.8 ± 2.3	6.2 ± 1.2
Data	54	47	7
	$E_{\mathrm{T}}^{\mathrm{miss}} > 60\,\mathrm{GeV}$	$E_{\mathrm{T}}^{\mathrm{miss}} > 80\,\mathrm{GeV}$	$E_{\mathrm{T}}^{\mathrm{miss}} > 100\,\mathrm{GeV}$
Z+jets bkg	5.7 ± 1.8	2.2 ± 0.9	0.6 ± 0.3
Flavor symmetric	2.4 ± 0.9	1.8 ± 0.7	1.6 ± 0.6
Other SM bkg	0.3 ± 0.2	0.3 ± 0.2	0.2 ± 0.1
Total SM bkg	8.5 ± 2.0	4.3 ± 1.2	2.4 ± 0.7
Data	8	2	0
hZ events			
$m_{\widetilde{\chi}_1^0} = 130\,\mathrm{GeV}$	5.4 ± 0.1	3.1 ± 0.1	1.7 ± 0.1
$m_{\widetilde{\chi}_1^0} = 150\,\mathrm{GeV}$	5.3 ± 0.1	3.3 ± 0.1	2.0 ± 0.1
$m_{\widetilde{\chi}_1^0} = 200\,\mathrm{GeV}$	4.7 ± 0.1	4.2 ± 0.1	3.3 ± 0.1
$m_{\widetilde{\chi}_1^0} = 250\,\mathrm{GeV}$	3.5 ± 0.1	3.2 ± 0.1	2.8 ± 0.1

8 Search in channels with three or more leptons or with a $\mathrm{ZZ} \to \ell^+\ell^-$+2 jets combination

The SUSY scenarios of interest to this study (Fig. 1) can yield events with three or more leptons if the h, Z, and W bosons decay leptonically. We therefore combine the results presented here with our results on final states with three or more leptons [35] to derive unified conclusions for these scenarios. The three-or-more-lepton results provide sensitivity to the SUSY ZZ channel, i.e., to events in which the two Higgs bosons in Fig. 1 (left) are each replaced by a Z boson. In contrast, the studies presented in Sections 5–7 have little sensitivity to ZZ production.

The analysis of Ref. [35] requires events to contain at least three charged lepton candidates including at most one hadronically decaying τ lepton (τ_{h}) candidate. The events are divided into exclusive categories based on the number and flavor of the leptons, the presence or absence of an opposite-sign, same-flavor lepton pair (OSSF), the invariant mass of the OSSF pair including its consistency with the Z boson mass, the presence or absence of a tagged b jet, the $E_{\mathrm{T}}^{\mathrm{miss}}$ value, and the H_{T} value. As in Ref. [35], we order the search channels by their expected sensitivities and, for the interpretation of results (Section 10), select channels starting with the most sensitive one, and do not consider additional channels once the expected number of signal events, integrated over the retained channels, equals or exceeds 90% of the total expected number.

The seven most sensitive channels for hh signal events, assuming a higgsino mass of $m_{\widetilde{\chi}_1^0} = 150\,\mathrm{GeV}$ and a $\widetilde{\chi}_1^0 \to \mathrm{h}\widetilde{\mathrm{G}}$ branching fraction of unity, are presented in Table 6. Similar results are obtained for other values of the higgsino mass. Table 6 includes the observed numbers of events, the SM background estimates [35], and the predicted signal yields. Some excess in the data relative to the expectation is seen for the last two channels listed in the table, for which

Table 6: The seven most sensitive search channels of the three-or-more lepton analysis [35] for the $\widetilde{\chi}_1^0(\rightarrow \mathrm{h}\widetilde{\mathrm{G}})\widetilde{\chi}_1^0(\rightarrow \mathrm{h}\widetilde{\mathrm{G}})$ di-higgsino production scenario assuming a higgsino mass of 150 GeV and an LSP (gravitino) mass of 1 GeV. For all channels, $H_\mathrm{T} < 200$ GeV and the number of tagged b jets is zero. The symbols N_ℓ, N_{τ_h}, and N_OSSF indicate the number of charged leptons, hadronically decaying τ-lepton candidates, and opposite-sign same-flavor (OSSF) lepton pairs, respectively. "Below-Z" means that the invariant mass $m_{\ell\ell}$ of the OSSF pair (if present) lies below the region of the Z boson ($m_{\ell\ell} < 75$ GeV), while "Off-Z" means that either $m_{\ell\ell} < 75$ GeV or $m_{\ell\ell} > 105$ GeV. The uncertainties shown for the SM background estimates are the combined statistical and systematic terms, while those shown for signal events are statistical. The channels are ordered according to the values of N_ℓ, N_{τ_h}, N_OSSF, and $E_\mathrm{T}^\mathrm{miss}$.

N_ℓ	N_{τ_h}	N_OSSF	$m_{\ell\ell}$ range	$E_\mathrm{T}^\mathrm{miss}$ (GeV)	SM background	Data	hh events, $m_{\widetilde{\chi}_1^0} = 150$ GeV
3	0	0	—	0-50	51 ± 11	53	3.1 ± 0.6
3	0	0	—	50-100	38 ± 15	35	2.7 ± 0.6
3	0	1	Below-Z	50-100	130 ± 27	142	7.4 ± 1.6
3	1	0	—	50-100	400 ± 150	406	8.0 ± 1.4
4	0	1	Off-Z	50-100	0.2 ± 0.1	0	0.5 ± 0.2
4	1	1	Off-Z	0-50	7.5 ± 2.0	15	0.8 ± 0.2
4	1	1	Off-Z	50-100	2.1 ± 0.5	4	0.7 ± 0.2

15 and 4 events are observed, compared to 7.5 ± 2.0 and 2.1 ± 0.5 events, respectively, that are expected. The combined local excess is 2.6 standard deviations. The excesses in these two search channels are discussed in Ref. [35], where it is demonstrated that they are consistent with a statistical fluctuation once the large number of the search channels in the analysis is taken into account ("look-elsewhere effect").

We also make use of our results [36] on final states with two or more jets and either a $\mathrm{Z} \rightarrow \mathrm{e}^+\mathrm{e}^-$ or $\mathrm{Z} \rightarrow \mu^+\mu^-$ decay, which provide yet more sensitivity to the SUSY ZZ channel. In the study of Ref. [36], events must contain either an $\mathrm{e}^+\mathrm{e}^-$ or $\mu^+\mu^-$ pair and no other lepton, at least two jets, no tagged b jets, and large values of $E_\mathrm{T}^\mathrm{miss}$. The invariant mass of the lepton pair, and the dijet mass formed from the two jets with highest p_T values, are both required to be consistent with the Z boson mass. Ref. [36] also contains results on the hW signal scenario of Fig. 1 (right) in decay channels that are complementary to those considered here. We make use of these results in our interpretation of the hW scenario.

9 Systematic uncertainties

Systematic uncertainties for the various background estimates are presented in the respective sections above, or, in the case of the studies mentioned in Section 8, in Refs. [35, 36].

Systematic uncertainties associated with the selection efficiency for signal events arise from various sources. The uncertainties related to the jet energy scale, jet energy resolution, pileup modeling, trigger efficiencies, b-jet tagging efficiency correction factors, lepton identification and isolation criteria, and the modeling of initial-state radiation (ISR), are evaluated by varying the respective quantities by their uncertainties, while those associated with the parton distribution functions are determined [66, 75, 76] using the recommendations of Ref. [77]. The uncertainty of the luminosity determination is 2.6% [78]. Table 7 lists typical values of these uncertainties. In setting limits (Section 10), correlations between systematic uncertainties across the different search channels are taken into account.

Table 7: Typical values of the systematic uncertainty for signal efficiency, in percentage.

Source	
Jet energy scale	5-10%
Jet energy resolution	2-4%
Pileup modeling	4%
Trigger efficiency	1-5%
b-jet tagging efficiency	5-10%
Lepton identification and isolation	5%
ISR modeling	1%
Parton distribution functions	1%
Luminosity	2.6%

10 Interpretation

In this section, we present the interpretation of our results. We set 95% confidence level (CL) upper limits on the production cross sections of the considered scenarios using a modified frequentist CL_S method based on the LHC-style test statistic [79–81]. The input to the procedure is the number of observed events, the number of expected SM background events (with uncertainties), and the number of predicted signal events in each bin of the distributions of Figs. 5, 7 (right), 8 (right), 10, and 12, as well as the relevant results from Refs. [35, 36] (see Tables 2–3 of Ref. [35] and Tables 4–6 of Ref. [36]). The cross section upper limits are compared to the predicted cross sections, which have uncertainties [77] of approximately 5%.

We first present upper limits for the GMSB di-higgsino NLSP model [28, 34] discussed in the introduction. The limits are presented as a function of the $\widetilde{\chi}_1^0$ higgsino mass for the hh, ZZ, and hZ topologies separately and then in the two-dimensional plane of the $\widetilde{\chi}_1^0 \to \mathrm{h}\widetilde{\mathrm{G}}$ branching fraction versus $m_{\widetilde{\chi}_1^0}$. We assume that the higgsino $\widetilde{\chi}_1^0$ can decay only to the $\mathrm{h}\widetilde{\mathrm{G}}$ or $\mathrm{Z}\widetilde{\mathrm{G}}$ states. Following our discussion of the GMSB model, we present limits for the electroweak chargino-neutralino pair production process of Fig. 1 (right) as a function of the LSP ($\widetilde{\chi}_1^0$) and common $\widetilde{\chi}_2^0$, $\widetilde{\chi}_1^\pm$ masses, taking the $\widetilde{\chi}_2^0 \to \mathrm{h}\widetilde{\chi}_1^0$ and $\widetilde{\chi}_1^\pm \to \mathrm{W}^\pm\widetilde{\chi}_1^0$ branching fractions each to be 1.0.

10.1 Limits on the GMSB di-higgsino NLSP model

10.1.1 The hh topology

Figure 13 (top) shows the 95% CL cross section upper limits on higgsino pair production through the hh channel [Fig. 1 (left)], i.e., assuming the $\widetilde{\chi}_1^0 \to \mathrm{h}\widetilde{\mathrm{G}}$ branching fraction to be unity. The limits are derived using the combined results from the $\mathrm{hh} \to \mathrm{b\bar{b}b\bar{b}}$, $\gamma\gamma\mathrm{b\bar{b}}$, $\gamma\gamma$+leptons, and three-or-more-lepton studies, corresponding to the results presented in Sections 5, 6.1, 6.3, and 8, respectively. Both the expected and observed limits are shown, where the expected limits are derived from the SM background estimates. The expected results are presented with one, two, and three standard deviation bands of the experimental uncertainties, which account for the uncertainties of the background prediction and for the statistical uncertainties of the signal observables. The NLO+NLL theoretical cross section [38, 62, 63] with its one standard deviation uncertainty band is also shown. Results for the individual search channels are presented in Fig. 13 (bottom).

It is seen that the expected exclusion region lies near the predicted di-higgsino cross section (within about one standard deviation of the experimental uncertainties) for higgsino mass values below around 360 GeV. Most of this sensitivity is provided by the $\mathrm{hh} \to \mathrm{b\bar{b}b\bar{b}}$ channel, which dominates the results for $m_{\widetilde{\chi}_1^0} \gtrsim 200$ GeV. For lower mass values, the $\gamma\gamma\mathrm{b\bar{b}}$ and three-or-

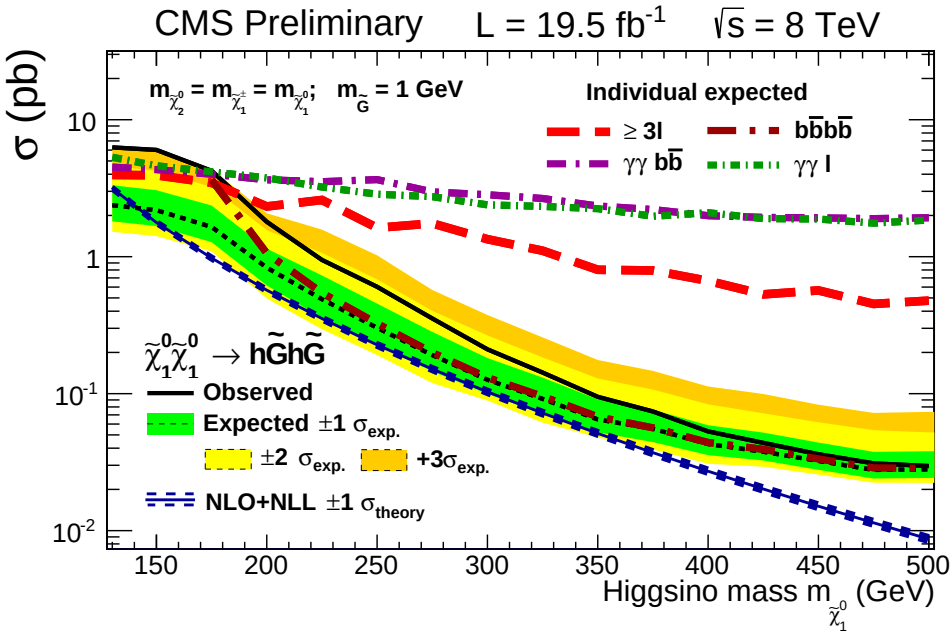

Figure 13: Observed and expected 95% confidence level (CL) upper limits on the cross section for higgsino pair production in the hh topology as a function of the higgsino mass for the combined $\mathrm{b\bar{b}b\bar{b}}$, $\gamma\gamma\mathrm{b\bar{b}}$, $\gamma\gamma$+leptons, and three-or-more lepton channels. The green, yellow, and orange bands indicate the one-, two-, and three-standard-deviation uncertainty intervals, respectively, for the expected results. The theoretical cross section and the expected curves for the individual search channels are also shown.

more-lepton channels provide the greatest sensitivity. The $\mathrm{hh} \to \mathrm{b\bar{b}b\bar{b}}$ channel loses sensitivity for $m_{\tilde{\chi}_1^0} \lesssim 200\,\mathrm{GeV}$ because the S_{MET} spectrum of signal events becomes similar to the spectrum from SM events.

The observed limits in Fig. 13 are seen to deviate from the expected ones by slightly more than three standard deviations for $m_{\tilde{\chi}_1^0} \lesssim 170\,\mathrm{GeV}$. The main contribution to this excess (2.6 standard deviations, discussed in Section 8) arises from the three-or-more-lepton channel, and was also reported in Ref. [35]. The electron (but not muon) component of the $\gamma\gamma$+leptons channel also contributes to this excess, which is apparent in the $30 < M_{\mathrm{T}} < 90\,\mathrm{GeV}$ region of Fig. 10 (right). Since the excess in this channel is not large (2.1 standard deviations), is not signal-like [for the $E_{\mathrm{T}}^{\mathrm{miss}}$ distribution, the excess of data events above the SM background prediction clusters at low values $E_{\mathrm{T}}^{\mathrm{miss}} \lesssim 30\,\mathrm{GeV}$, as seen in Fig. 19 (right)], and since there is not a corresponding excess in the muon channel, we consider the excess seen in Fig. 10 (right) to be consistent with a statistical fluctuation.

10.1.2 The ZZ and hZ topologies

The 95% CL cross section upper limits on higgsino pair production through the ZZ channel are presented in Fig. 14 (top). For these results, we assume the $\tilde{\chi}_1^0 \to \mathrm{Z}\tilde{\mathrm{G}}$ branching fraction to be unity. These results are derived using the two search channels that dominate the sensitivity to the ZZ topology: the three-or-more-lepton and $\ell^+\ell^-$+2 jets channels (Section 8). In the context of this scenario, higgsino masses below around 380 GeV are excluded.

To illustrate the sensitivity of our analysis to the hZ topology [Fig. 1 (middle)], we assume the $\tilde{\chi}_1^0 \to \mathrm{h}\tilde{\mathrm{G}}$ and $\tilde{\chi}_1^0 \to \mathrm{Z}\tilde{\mathrm{G}}$ branching fractions each to be 0.5 and ignore contributions from the hh and ZZ channels. Figure 14 (bottom) shows the 95% CL cross section upper limits for

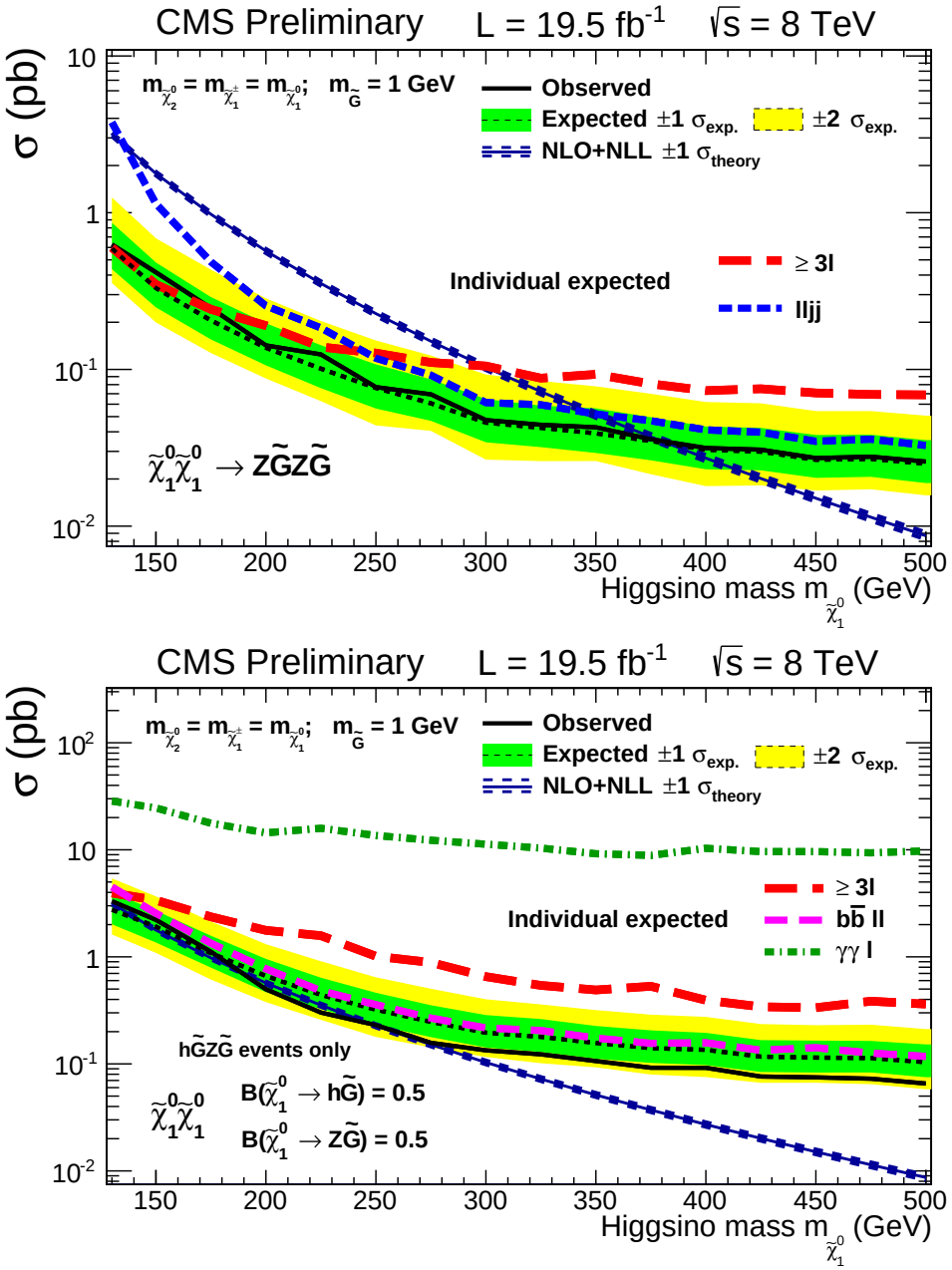

Figure 14: (top) Observed and expected 95% confidence level (CL) upper limits on the cross section for higgsino pair production in the ZZ topology as a function of the higgsino mass for the combined three-or-more lepton and $\ell^+\ell^-$+2 jets channels. The green and yellow bands indicate the one- and two-standard-deviation uncertainty intervals, respectively, for the expected results. The theoretical cross section and the expected curves for the individual search channels are also shown. (bottom) Corresponding results for the hZ topology, assuming the $\widetilde{\chi}_1^0 \to h\widetilde{G}$ and $\widetilde{\chi}_1^0 \to Z\widetilde{G}$ branching fractions each to be 0.5, ignoring contributions from hh and ZZ events, for the individual and combined $\gamma\gamma$+leptons, $b\bar{b}\ell^+\ell^-$, and three-or-more-lepton channels.

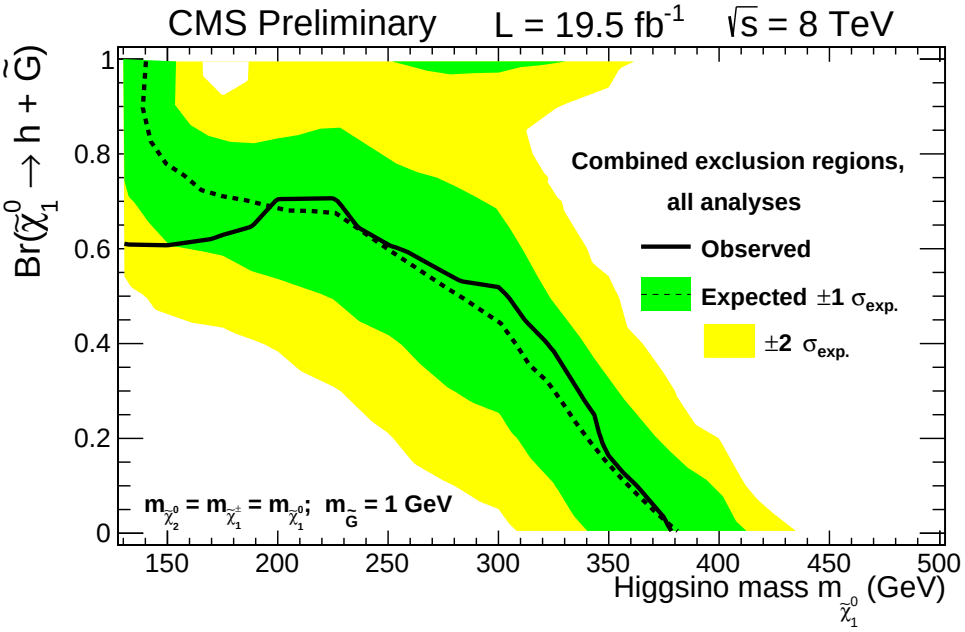

Figure 15: Observed and expected 95% confidence level (CL) exclusion regions for higgsino pair production, with all channels combined, in the plane of the higgsino branching fraction to a Higgs boson and LSP, versus the higgsino mass. The green and yellow bands indicate the one- and two-standard-deviation uncertainty intervals, respectively. The excluded regions correspond to the area below the contours.

the hZ topology derived from the combined $\gamma\gamma$+leptons, $\mathrm{b\bar{b}}\ell^+\ell^-$, and three-or-more-lepton samples (Sections 6.3, 7, and 8, respectively). The results are dominated by the $\mathrm{b\bar{b}}\ell^+\ell^-$ channel. The three-or-more-lepton channel contributes mainly for higgsino mass values below around 170 GeV. The sensitivity of the $\gamma\gamma$+leptons channel is minimal. [The $\gamma\gamma$+2 jets channel also contributes minimally and is not included in the combination of Fig. 14 (bottom).]

10.1.3 Exclusion region as a function of the $\tilde{\chi}_1^0$ mass and $\tilde{\chi}_1^0 \to \mathrm{h}\tilde{\mathrm{G}}$ branching fraction

Figure 15 presents the 95% CL exclusion region for the GMSB di-higgsino NLSP scenario in the two-dimensional plane of the $\tilde{\chi}_1^0 \to \mathrm{h}\tilde{\mathrm{G}}$ higgsino branching fraction versus the higgsino mass $m_{\tilde{\chi}_1^0}$. The results are based on all relevant studies discussed in this paper including those of Refs. [35, 36]. The combined results exclude a significant fraction of the plane. For higgsino mass values above around 200 GeV, the observed results are in agreement with the expected ones within one standard deviation of the uncertainties. For smaller higgsino mass values, the observed exclusion boundary lies below the expected one because of the excesses in data discussed in Section 10.1.1. Horizontal slices of Fig. 15 at branching fractions of one and zero correspond to the results presented in Figs. 13 and 14 (top) for the hh and ZZ topologies, respectively. The corresponding results for a horizontal slice at a branching fraction of 0.5 are shown in Fig. 16.

To illustrate the relative importance of the different search channels for the results of Fig. 15, we present in Fig. 17 the observed and expected exclusion regions when each principal component of the analysis is in turn removed from the combination. For this purpose, the $\mathrm{h} \to \gamma\gamma$ studies of Section 6 are grouped together into a "$\gamma\gamma$+X" category, and the $\mathrm{h}(\to \mathrm{b\bar{b}})\mathrm{Z}(\to \ell^+\ell^-)$ and $\mathrm{Z}(\to \ell^+\ell^-)\mathrm{Z}(\to 2\,\text{jets})$ studies of Sections 7 and 8 into a "$\ell\ell$+X" category. The greatest impact is from the three-or-more lepton and combined $\mathrm{b\bar{b}}\ell^+\ell^-$ and $\ell^+\ell^-$+2 jets channels, because of

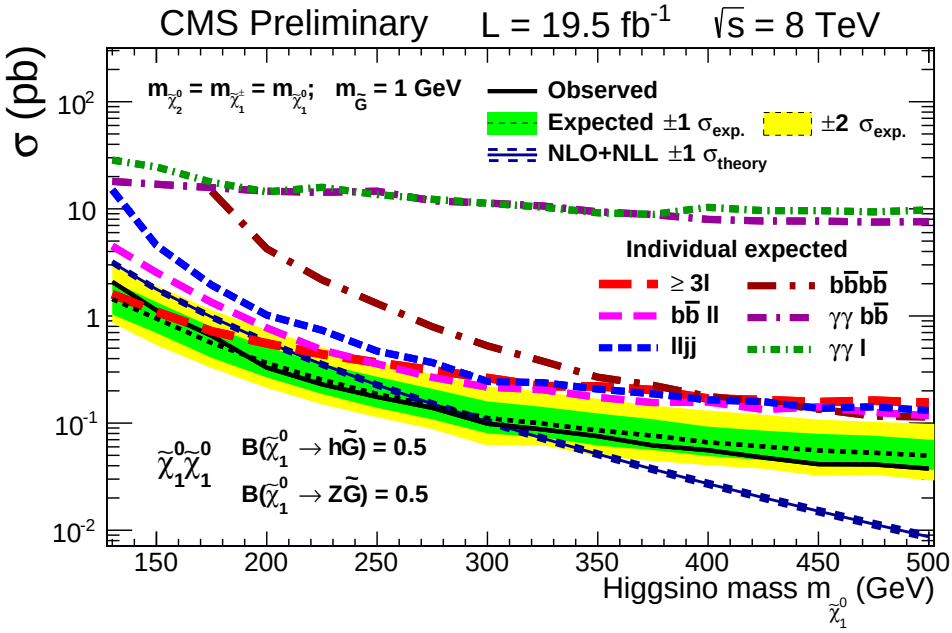

Figure 16: Observed and expected 95% confidence level (CL) upper limits on the cross section for higgsino pair production as a function of the higgsino mass assuming the $\widetilde{\chi}_1^0 \to \mathrm{h}\widetilde{\mathrm{G}}$ and $\widetilde{\chi}_1^0 \to \mathrm{Z}\widetilde{\mathrm{G}}$ branching fractions each to be 0.5, including contributions from hh and ZZ events, for the combined $\mathrm{b\bar{b}b\bar{b}}$, $\gamma\gamma\mathrm{b\bar{b}}$, $\gamma\gamma$+leptons, $\mathrm{b\bar{b}}\ell^+\ell^-$, three-or-more lepton, and $\ell^+\ell^-$+2 jets channels. The green and yellow bands indicate the one- and two-standard-deviation uncertainty intervals, respectively, for the expected results. The theoretical cross section and the expected curves for the individual search channels are also shown.

the stringent constraints they impose on ZZ production [Fig. 14 (top)]. A distribution showing which search channel provides the most stringent 95% CL cross section upper limit in the plane of the $\widetilde{\chi}_1^0$ branching fraction versus the $\widetilde{\chi}_1^0$ mass is presented in Fig. 20 of Appendix A.

10.2 The hW topology

In Ref. [36], we present limits on the chargino-neutralino pair-production scenario of Fig. 1 (right), i.e., on a generic new-physics SUSY-like process with a Higgs boson, a W boson, and $E_{\mathrm{T}}^{\mathrm{miss}}$. The event signatures considered are those that yield a single electron or muon and a $\mathrm{b\bar{b}}$ pair, a same-sign ee, $\mu\mu$, or eμ pair and no third charged lepton, and three or more charged leptons [35]. These results target the $\mathrm{h}(\to \mathrm{b\bar{b}})\mathrm{W}(\to \ell\nu)$ and $\mathrm{h}(\to \mathrm{ZZ}, \mathrm{WW}, \tau\tau)\mathrm{W}(\to \ell\nu)$ channels, with ℓ an electron, muon, or leptonically decaying τ lepton. With the present work, we add the search channels with $\mathrm{h} \to \gamma\gamma$ and either $\mathrm{W} \to 2$ jets or $\mathrm{W} \to \ell\nu$, corresponding to the studies of Sections 6.2 and 6.3.

The 95% CL upper bounds on the chargino-neutralino cross section based on the combination of results from Ref. [36] with the two $\gamma\gamma$ search channels considered here are shown in Fig. 18. The top plot shows the cross section limits in the LSP versus $\widetilde{\chi}_2^0 = \widetilde{\chi}_1^\pm$ mass plane. The bottom plot shows the limits as a function of the $\widetilde{\chi}_2^0 = \widetilde{\chi}_1^\pm$ mass assuming an LSP mass of $m_{\widetilde{\chi}_1^0} = 1\,\mathrm{GeV}$. The single most sensitive channel is the single-lepton search from Ref. [36].

For small values of the LSP mass, we exclude chargino-neutralino pair production for $\widetilde{\chi}_2^0 = \widetilde{\chi}_1^\pm$ mass values up to 210 GeV, based on the theoretical prediction for the cross section minus one standard deviation of its uncertainty. This represents a modest improvement of about 5% compared to the corresponding result in Ref. [36]. The individual diphoton cross section results

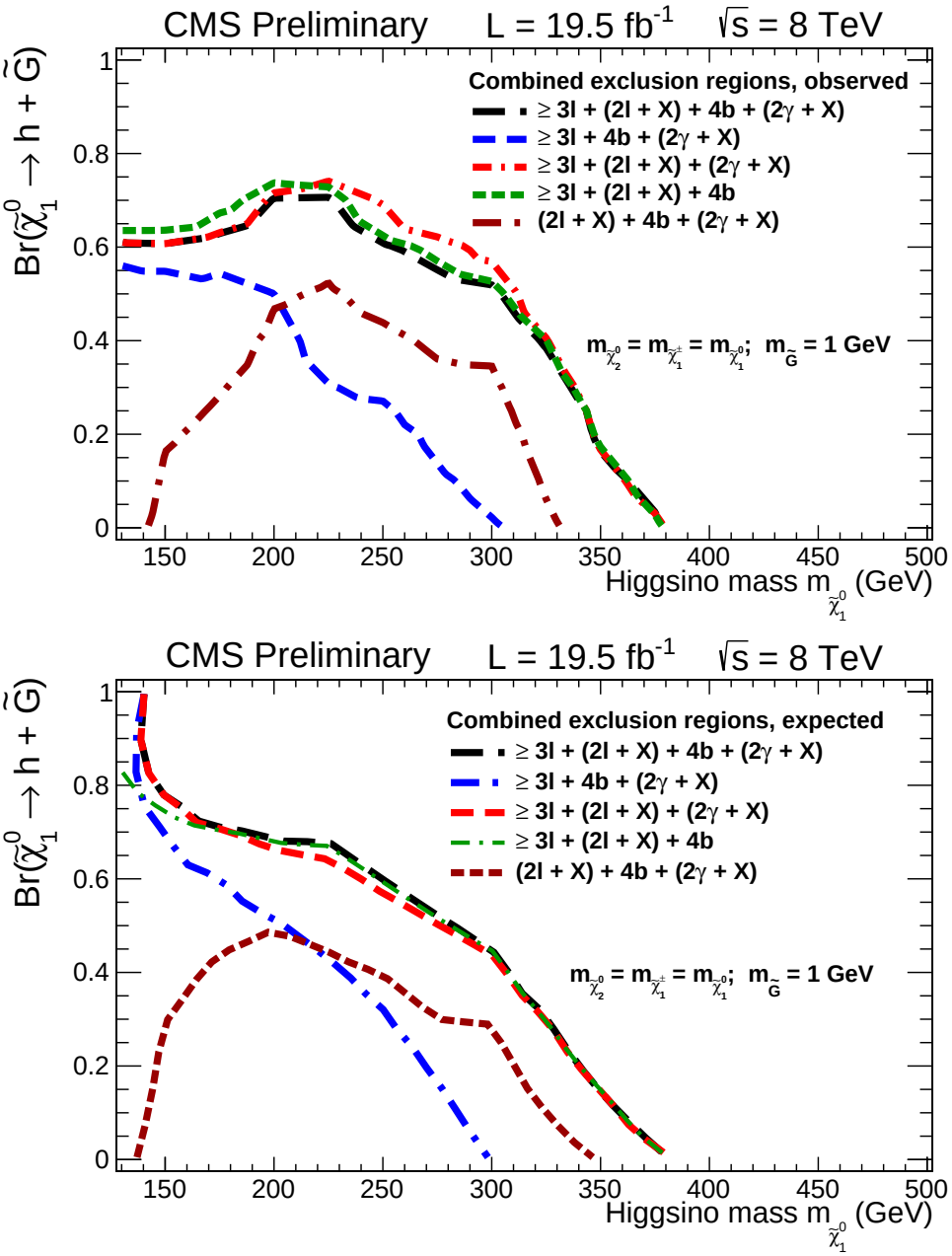

Figure 17: (top) Observed, and (bottom) expected 95% confidence level (CL) exclusion regions for higgsino pair production in the plane of the higgsino branching fraction to a Higgs boson and the LSP, versus the higgsino mass, with each principal search channel group removed in turn from the combination. The excluded regions correspond to the area below the contours.

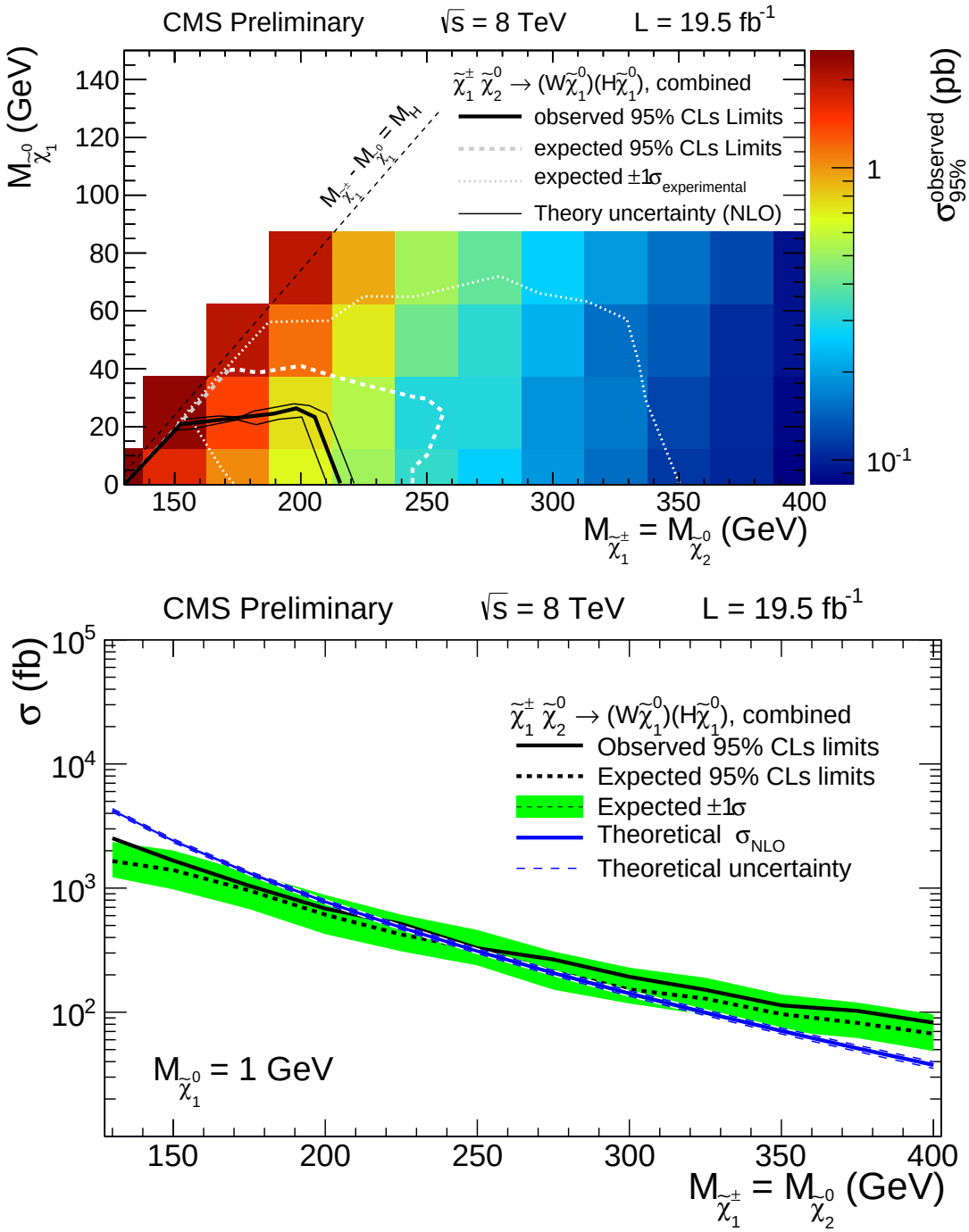

Figure 18: (top) Observed and expected 95% confidence level (CL) upper limits on the cross section for electroweak chargino-neutralino $\tilde{\chi}_1^{\pm}\tilde{\chi}_2^0$ pair production (with $m_{\tilde{\chi}_1^{\pm}} = m_{\tilde{\chi}_2^0}$) as a function of the LSP and $\tilde{\chi}_2^0$ masses for the combined results on single-lepton, same-sign dilepton, and multilepton data from Ref. [36] with the diphoton data presented here. (bottom) Corresponding results as a function of the $\tilde{\chi}_2^0$ mass for an LSP mass of 1 GeV. The green band indicates the one-standard-deviation interval. The theoretical cross section is also shown.

assuming $m_{\widetilde{\chi}_1^0} = 1\,\text{GeV}$ are presented in Fig. 21 of Appendix A.

11 Summary

A search is presented for the electroweak pair production of higgsinos ($\widetilde{\chi}_1^0$) in proton-proton collisions at 8 TeV, based on the gauge-mediated-SUSY-breaking scenario of Ref. [28]. Each higgsino is presumed to decay to a Higgs boson (h) and the lightest supersymmetric particle (LSP), which escapes without detection, or else to a Z boson and an LSP, where the LSP is an almost massless gravitino $\widetilde{\text{G}}$. We search for an excess, relative to the expectation from standard model processes, of events with an hh, hZ, or ZZ boson pair produced in association with a large value of either missing transverse energy $E_{\text{T}}^{\text{miss}}$, transverse mass M_{T}, or the scalar sum S_{T}^{h} of the two boson transverse momenta, depending on the search channel. In addition, we perform a search for electroweak chargino-neutralino ($\widetilde{\chi}_1^{\pm}\widetilde{\chi}_2^0$) pair production in channels with an hW boson pair and $E_{\text{T}}^{\text{miss}}$. In this case, the LSP is a massive neutralino, also denoted $\widetilde{\chi}_1^0$. The assumed decay modes are $\widetilde{\chi}_1^{\pm} \to \text{W}\widetilde{\chi}_1^0$ and $\widetilde{\chi}_2^0 \to \text{h}\widetilde{\chi}_1^0$. The data sample, collected with the CMS detector at the LHC in 2012, corresponds to an integrated luminosity of about $19.5\,\text{fb}^{-1}$.

We select events with four bottom-quark jets (b jets), events with two b jets and two photons, and events with two b jets and an $\ell^+\ell^-$ pair (with ℓ an electron or muon), providing sensitivity to the $\text{h}(\to \text{b}\overline{\text{b}})\text{h}(\to \text{b}\overline{\text{b}})$, $\text{h}(\to \gamma\gamma)\text{h}(\to \text{b}\overline{\text{b}})$, and $\text{h}(\to \text{b}\overline{\text{b}})\text{Z}(\to \ell^+\ell^-)$ channels, respectively. We also select events with two photons accompanied by two light-quark jets, and events with two photons accompanied by at least one electron or muon, providing sensitivity to the $\text{h}(\to \gamma\gamma)\text{Z}/\text{W}(\to 2\,\text{jets})$ channels, and to the $\text{h}(\to \gamma\gamma)\text{h}(\to \text{ZZ}/\text{WW}/\tau\tau)$ and $\text{h}(\to \gamma\gamma)\text{Z}/\text{W}$ channels where the Z and W bosons decay leptonically. As an aid for studies of signal scenarios other than those considered in this paper, Appendix B provides tables of signal yields at different stages of the event selection process for the studies presented herein. We incorporate results from Refs. [35] and [36] to gain sensitivity to di-higgsino events in the ZZ channel and to access complementary $\widetilde{\chi}_1^{\pm}\widetilde{\chi}_2^0$ decay modes.

The results are combined in a likelihood fit to derive 95% confidence level upper limits on the di-higgsino production cross section in the two-dimensional plane of the higgsino branching fraction to the $\text{h}\widetilde{\text{G}}$ state versus the higgsino mass $m_{\widetilde{\chi}_1^0}$, where $\widetilde{\chi}_1^0 \to \text{h}\widetilde{\text{G}}$ and $\widetilde{\chi}_1^0 \to \text{Z}\widetilde{\text{G}}$ are taken as the only possible higgsino decay modes. With the $\widetilde{\chi}_1^0 \to \text{Z}\widetilde{\text{G}}$ branching fraction set to unity, higgsinos with a mass value below 380 GeV are excluded. With the $\widetilde{\chi}_1^0 \to \text{h}\widetilde{\text{G}}$ branching fraction set to unity, higgsinos are not excluded for any mass value but we obtain an expected exclusion region within about one standard deviation of the experimental uncertainties from the predicted di-higgsino cross section for higgsino mass values below around 360 GeV.

We also determine 95% confidence level upper limits on the cross section for electroweak chargino-neutralino $\widetilde{\chi}_1^{\pm}\widetilde{\chi}_2^0$ pair production, adding the search channels with $\text{h} \to \gamma\gamma$ and either $\text{W} \to 2$ jets or $\text{W} \to \ell\nu$ to the results presented in Ref. [36]. For small values of the LSP mass, we exclude this process for chargino mass values up to 210 GeV, where the $\widetilde{\chi}_1^{\pm}$ and $\widetilde{\chi}_2^0$ masses are taken to be equal.

Acknowledgements

We congratulate our colleagues in the CERN accelerator departments for the excellent performance of the LHC and thank the technical and administrative staffs at CERN and at other CMS institutes for their contributions to the success of the CMS effort. In addition, we gratefully

acknowledge the computing centres and personnel of the Worldwide LHC Computing Grid for delivering so effectively the computing infrastructure essential to our analyses. Finally, we acknowledge the enduring support for the construction and operation of the LHC and the CMS detector provided by the following funding agencies: the Austrian Federal Ministry of Science and Research and the Austrian Science Fund; the Belgian Fonds de la Recherche Scientifique, and Fonds voor Wetenschappelijk Onderzoek; the Brazilian Funding Agencies (CNPq, CAPES, FAPERJ, and FAPESP); the Bulgarian Ministry of Education and Science; CERN; the Chinese Academy of Sciences, Ministry of Science and Technology, and National Natural Science Foundation of China; the Colombian Funding Agency (COLCIENCIAS); the Croatian Ministry of Science, Education and Sport, and the Croatian Science Foundation; the Research Promotion Foundation, Cyprus; the Ministry of Education and Research, Recurrent financing contract SF0690030s09 and European Regional Development Fund, Estonia; the Academy of Finland, Finnish Ministry of Education and Culture, and Helsinki Institute of Physics; the Institut National de Physique Nucléaire et de Physique des Particules / CNRS, and Commissariat à l'Énergie Atomique et aux Énergies Alternatives / CEA, France; the Bundesministerium für Bildung und Forschung, Deutsche Forschungsgemeinschaft, and Helmholtz-Gemeinschaft Deutscher Forschungszentren, Germany; the General Secretariat for Research and Technology, Greece; the National Scientific Research Foundation, and National Innovation Office, Hungary; the Department of Atomic Energy and the Department of Science and Technology, India; the Institute for Studies in Theoretical Physics and Mathematics, Iran; the Science Foundation, Ireland; the Istituto Nazionale di Fisica Nucleare, Italy; the Korean Ministry of Education, Science and Technology and the World Class University program of NRF, Republic of Korea; the Lithuanian Academy of Sciences; the Ministry of Education, and University of Malaya (Malaysia); the Mexican Funding Agencies (CINVESTAV, CONACYT, SEP, and UASLP-FAI); the Ministry of Business, Innovation and Employment, New Zealand; the Pakistan Atomic Energy Commission; the Ministry of Science and Higher Education and the National Science Centre, Poland; the Fundação para a Ciência e a Tecnologia, Portugal; JINR, Dubna; the Ministry of Education and Science of the Russian Federation, the Federal Agency of Atomic Energy of the Russian Federation, Russian Academy of Sciences, and the Russian Foundation for Basic Research; the Ministry of Education, Science and Technological Development of Serbia; the Secretaría de Estado de Investigación, Desarrollo e Innovación and Programa Consolider-Ingenio 2010, Spain; the Swiss Funding Agencies (ETH Board, ETH Zurich, PSI, SNF, UniZH, Canton Zurich, and SER); the National Science Council, Taipei; the Thailand Center of Excellence in Physics, the Institute for the Promotion of Teaching Science and Technology of Thailand, Special Task Force for Activating Research and the National Science and Technology Development Agency of Thailand; the Scientific and Technical Research Council of Turkey, and Turkish Atomic Energy Authority; the National Academy of Sciences of Ukraine, and State Fund for Fundamental Researches, Ukraine; the Science and Technology Facilities Council, UK; the US Department of Energy, and the US National Science Foundation.

Individuals have received support from the Marie-Curie programme and the European Research Council and EPLANET (European Union); the Leventis Foundation; the A. P. Sloan Foundation; the Alexander von Humboldt Foundation; the Belgian Federal Science Policy Office; the Fonds pour la Formation à la Recherche dans l'Industrie et dans l'Agriculture (FRIA-Belgium); the Agentschap voor Innovatie door Wetenschap en Technologie (IWT-Belgium); the Ministry of Education, Youth and Sports (MEYS) of Czech Republic; the Council of Science and Industrial Research, India; the Compagnia di San Paolo (Torino); the HOMING PLUS programme of Foundation for Polish Science, cofinanced by EU, Regional Development Fund; and the Thalis and Aristeia programmes cofinanced by EU-ESF and the Greek NSRF.

References

[1] P. Ramond, "Dual theory for free fermions", *Phys. Rev. D* **3** (1971) 2415, doi:10.1103/PhysRevD.3.2415.

[2] Y. A. Golfand and E. P. Likhtman, "Extension of the algebra of Poincaré group generators and violation of P invariance", *JETP Lett.* **13** (1971) 323.

[3] A. Neveu and J. H. Schwarz, "Factorizable dual model of pions", *Nucl. Phys. B* **31** (1971) 86, doi:10.1016/0550-3213(71)90448-2.

[4] D. V. Volkov and V. P. Akulov, "Possible universal neutrino interaction", *JETP Lett.* **16** (1972) 438.

[5] J. Wess and B. Zumino, "A Lagrangian model invariant under supergauge transformations", *Phys. Lett. B* **49** (1974) 52, doi:10.1016/0370-2693(74)90578-4.

[6] J. Wess and B. Zumino, "Supergauge transformations in four dimensions", *Nucl. Phys. B* **70** (1974) 39, doi:10.1016/0550-3213(74)90355-1.

[7] P. Fayet, "Supergauge invariant extension of the Higgs mechanism and a model for the electron and its neutrino", *Nucl. Phys. B* **90** (1975) 104, doi:10.1016/0550-3213(75)90636-7.

[8] H. P. Nilles, "Supersymmetry, supergravity and particle physics", *Phys. Rept.* **110** (1984) 1, doi:10.1016/0370-1573(84)90008-5.

[9] H. E. Haber and G. L. Kane, "The search for supersymmetry: probing physics beyond the standard model", *Phys. Rept.* **117** (1985) 75, doi:10.1016/0370-1573(85)90051-1.

[10] G. R. Farrar and P. Fayet, "Phenomenology of the production, decay, and detection of new hadronic states associated with supersymmetry", *Phys. Lett. B* **76** (1978) 575, doi:10.1016/0370-2693(78)90858-4.

[11] ATLAS Collaboration, "Search for new phenomena in final states with large jet multiplicities and missing transverse momentum at $\sqrt{s} = 8$ TeV proton-proton collisions using the ATLAS experiment", *JHEP* **10** (2013) 130, doi:10.1007/JHEP10(2013)130, arXiv:1308.1841.

[12] ATLAS Collaboration, "Search for direct third-generation squark pair production in final states with missing transverse momentum and two b jets in $\sqrt{s} = 8$ TeV pp collisions with the ATLAS detector", *JHEP* **10** (2013) 189, doi:10.1007/JHEP10(2013)189, arXiv:1308.2631.

[13] ATLAS Collaboration, "Search for direct production of charginos and neutralinos in events with three leptons and missing transverse momentum in $\sqrt{s} = 8$ TeV pp collisions with the ATLAS detector", *JHEP* **04** (2014) 169, doi:10.1007/JHEP04(2014)169, arXiv:1402.7029.

[14] ATLAS Collaboration, "Search for direct top-squark pair production in final states with two leptons in pp collisions at $\sqrt{s} = 8$ TeV with the ATLAS detector", (2014). arXiv:1403.4853. Submitted to *JHEP*.

[15] ATLAS Collaboration, "Search for direct production of charginos, neutralinos and sleptons in final states with two leptons and missing transverse momentum in pp collisions at $\sqrt{s} = 8$ TeV with the ATLAS detector", (2014). arXiv:1403.5294. Submitted to *JHEP*.

[16] ATLAS Collaboration, "Search for supersymmetry in events with four or more leptons in $\sqrt{s} = 8$ TeV pp collisions with the ATLAS detector", (2014). arXiv:1405.5086. Submitted to *Phys. Rev. D*.

[17] CMS Collaboration, "Search for gluino mediated bottom- and top-squark production in multijet final states in pp collisions at 8 TeV", *Phys. Lett. B* **725** (2013) 243, doi:10.1016/j.physletb.2013.06.058, arXiv:1305.2390.

[18] CMS Collaboration, "Search for top-squark pair production in the single-lepton final state in pp collisions at $\sqrt{s} = 8$ TeV", *Eur. Phys. J. C* **73** (2013) 2677, doi:10.1140/epjc/s10052-013-2677-2, arXiv:1308.1586.

[19] CMS Collaboration, "Search for supersymmetry in pp collisions at $\sqrt{s} = 8$ TeV in events with a single lepton, large jet multiplicity, and multiple b jets", (2013). arXiv:1311.4937. Submitted to *Phys. Lett. B*.

[20] CMS Collaboration, "Search for new physics in events with same-sign dileptons and jets in pp collisions at $\sqrt{s} = 8$ TeV", *JHEP* **01** (2014) 163, doi:10.1007/JHEP01(2014)163, arXiv:1311.6736.

[21] CMS Collaboration, "Search for new physics in the multijet and missing transverse momentum final state in proton-proton collisions at $\sqrt{s} = 8$ TeV", *JHEP* **06** (2014) 055, doi:10.1007/JHEP06(2014)055, arXiv:1402.4770.

[22] CMS Collaboration, "Search for top-squark pairs decaying into Higgs or Z bosons in pp collisions at $\sqrt{s} = 8$ TeV", (2014). arXiv:1405.3886. Submitted to *Phys. Lett. B*.

[23] ATLAS Collaboration, "Observation of a new particle in the search for the standard model Higgs boson with the ATLAS detector at the LHC", *Phys. Lett. B* **716** (2012) 1, doi:10.1016/j.physletb.2012.08.020, arXiv:1207.7214.

[24] CMS Collaboration, "Observation of a new boson with mass near 125 GeV in pp collisions at $\sqrt{s}$ = 7 and 8 TeV", *JHEP* **06** (2013) 081, doi:10.1007/JHEP06(2013)081, arXiv:1303.4571.

[25] CMS Collaboration, "Observation of a new boson at a mass of 125 GeV with the CMS experiment at the LHC", *Phys. Lett. B* **716** (2012) 30, doi:10.1016/j.physletb.2012.08.021, arXiv:1207.7235.

[26] G. Branco et al., "Theory and phenomenology of two-Higgs-doublet models", *Phys. Rept.* **516** (2012) 1, doi:10.1016/j.physrep.2012.02.002, arXiv:1106.0034.

[27] S. P. Martin, "A supersymmetry primer", (1997). arXiv:hep-ph/9709356.

[28] K. T. Matchev and S. D. Thomas, "Higgs and Z boson signatures of supersymmetry", *Phys. Rev. D* **62** (2000) 077702, doi:10.1103/PhysRevD.62.077702, arXiv:hep-ph/9908482.

[29] M. Asano, H. D. Kim, R. Kitano, and Y. Shimizu, "Natural supersymmetry at the LHC", *JHEP* **12** (2010) 019, doi:10.1007/JHEP12(2010)019, arXiv:1010.0692.

[30] Y. Kats, P. Meade, M. Reece, and D. Shih, "The Status of GMSB After 1/fb at the LHC", *JHEP* **02** (2012) 115, doi:10.1007/JHEP02(2012)115, arXiv:1110.6444.

[31] H. Baer et al., "Wh plus missing-$E_{\mathrm{T}}^{\mathrm{miss}}$ signature from gaugino pair production at the LHC", *Phys. Rev. D* **85** (2012) 055022, doi:10.1103/PhysRevD.85.055022, arXiv:1201.2949.

[32] P. Byakti and D. Ghosh, "Magic messengers in gauge mediation and signal for 125 GeV boosted Higgs boson", *Phys. Rev. D* **86** (2012) 095027, doi:10.1103/PhysRevD.86.095027, arXiv:1204.0415.

[33] K. Howe and P. Saraswat, "Excess Higgs production in neutralino decays", *JHEP* **10** (2012) 065, doi:10.1007/JHEP10(2012)065, arXiv:1208.1542.

[34] J. T. Ruderman and D. Shih, "General neutralino NLSPs at the early LHC", *JHEP* **08** (2012) 159, doi:10.1007/JHEP08(2012)159, arXiv:1103.6083.

[35] CMS Collaboration, "Search for anomalous production of events with three or more leptons in pp collisions at $\sqrt{s} = 8$ TeV", (2014). arXiv:1404.5801. Submitted to *Phys. Rev. D*.

[36] CMS Collaboration, "Searches for electroweak production of charginos, neutralinos, and sleptons decaying to leptons and W, Z, and Higgs bosons in pp collisions at 8 TeV", (2014). arXiv:1405.7570. Submitted to *Eur. Phys. J. C*.

[37] G. Giudice and R. Rattazzi, "Theories with gauge mediated supersymmetry breaking", *Phys. Rept.* **322** (1999) 419, doi:10.1016/S0370-1573(99)00042-3, arXiv:hep-ph/9801271.

[38] W. Beenakker et al., "The production of charginos/neutralinos and sleptons at hadron colliders", *Phys. Rev. Lett.* **83** (1999) 3780, doi:10.1103/PhysRevLett.100.029901,10.1103/PhysRevLett.83.3780, arXiv:hep-ph/9906298.

[39] CMS Collaboration, "The CMS experiment at the CERN LHC", *JINST* **3** (2008) S08004, doi:10.1088/1748-0221/3/08/S08004.

[40] CMS Collaboration, "Particle flow event reconstruction in CMS and performance for jets, taus and $E_{\mathrm{T}}^{\mathrm{miss}}$", CMS Physics Analysis Summary CMS-PAS-PFT-09-001, 2009.

[41] CMS Collaboration, "Commissioning of the particle-flow event reconstruction with the first LHC collisions recorded in the CMS detector", CMS Physics Analysis Summary CMS-PAS-PFT-10-001, 2010.

[42] CMS Collaboration, "Performance of tau-lepton reconstruction and identification in CMS", *JINST* **7** (2012) P01001, doi:10.1088/1748-0221/7/01/P01001, arXiv:1109.6034.

[43] M. Cacciari, G. P. Salam, and G. Soyez, "The anti-k_t jet clustering algorithm", *JHEP* **04** (2008) 063, doi:10.1088/1126-6708/2008/04/063, arXiv:0802.1189.

[44] M. Cacciari, G. P. Salam, and G. Soyez, "FastJet user manual", *Eur. Phys. J. C* **72** (2012) 1896, doi:10.1140/epjc/s10052-012-1896-2, arXiv:1111.6097.

[45] M. Cacciari and G. P. Salam, "Pileup subtraction using jet areas", *Phys. Lett. B* **659** (2008) 119, doi:10.1016/j.physletb.2007.09.077, arXiv:0707.1378.

[46] CMS Collaboration, "Missing transverse energy performance of the CMS detector", *JINST* **6** (2011) P09001, doi:10.1088/1748-0221/6/09/P09001, arXiv:1106.5048.

[47] CMS Collaboration, "Identification of b-quark jets with the CMS experiment", *JINST* **8** (2013) P04013, doi:10.1088/1748-0221/8/04/P04013, arXiv:1211.4462.

[48] CMS Collaboration, "Performance of b tagging at $\sqrt{s} = 8$ TeV in multijet, $\mathrm{t\bar{t}}$ and boosted topology events,", CMS Physics Analysis Summary CMS-PAS-BTV-13-001, 2013.

[49] J. Alwall et al., "MadGraph5: going beyond", *JHEP* **06** (2011) 128, doi:10.1007/JHEP06(2011)128, arXiv:1106.0522.

[50] S. Frixione, P. Nason, and C. Oleari, "Matching NLO QCD computations with parton shower simulations: the POWHEG method", *JHEP* **11** (2007) 070, doi:10.1088/1126-6708/2007/11/070, arXiv:0709.2092.

[51] T. Sjöstrand, S. Mrenna, and P. Skands, "PYTHIA 6.4 physics and manual", *JHEP* **05** (2006) 026, doi:10.1088/1126-6708/2006/05/026, arXiv:hep-ph/0603175.

[52] S. Frixione and B. R. Webber, "Matching NLO QCD computations and parton shower simulations", *JHEP* **06** (2002) 029, doi:10.1088/1126-6708/2002/06/029, arXiv:hep-ph/0204244.

[53] S. Frixione, P. Nason, and B. R. Webber, "Matching NLO QCD and parton showers in heavy flavor production", *JHEP* **08** (2003) 007, doi:10.1088/1126-6708/2003/08/007, arXiv:hep-ph/0305252.

[54] N. Kidonakis, "Differential and total cross sections for top pair and single top production", (2012). arXiv:1205.3453.

[55] J. M. Campbell and R. K. Ellis, "$\mathrm{t\bar{t}W^{\pm}}$ production and decay at NLO", *JHEP* **07** (2012) 052, doi:10.1007/JHEP07(2012)052, arXiv:1204.5678.

[56] M. Garzelli, A. Kardos, C. Papadopoulos, and Z. Trocsanyi, "$\mathrm{t\bar{t}W^{\pm}}$ and $\mathrm{t\bar{t}Z}$ hadroproduction at NLO accuracy in QCD with parton shower and hadronization effects", *JHEP* **11** (2012) 056, doi:10.1007/JHEP11(2012)056, arXiv:1208.2665.

[57] J. M. Campbell, R. K. Ellis, and C. Williams, "Vector boson pair production at the LHC", *JHEP* **07** (2011) 018, doi:10.1007/JHEP07(2011)018, arXiv:1105.0020.

[58] R. Gavin, Y. Li, F. Petriello, and S. Quackenbush, "W Physics at the LHC with FEWZ 2.1", *Comput. Phys. Commun.* **184** (2013) 208, doi:10.1016/j.cpc.2012.09.005, arXiv:1201.5896.

[59] S. Agostinelli et al., "GEANT4 — a simulation toolkit", *Nucl. Instr. and Meth. A* **506** (2003) 250, doi:10.1016/S0168-9002(03)01368-8.

[60] CMS Collaboration, "Measurement of the properties of a Higgs boson in the four-lepton final state", (2013). arXiv:1312.5353. In press in *Phys. Rev. D*.

[61] CMS Collaboration, "The fast simulation of the CMS detector at LHC", *J. Phys. Conf. Ser.* **331** (2011) 032049, doi:10.1088/1742-6596/331/3/032049.

[62] B. Fuks, M. Klasen, D. R. Lamprea, and M. Rothering, "Gaugino production in proton-proton collisions at a center-of-mass energy of 8 TeV", *JHEP* **10** (2012) 081, doi:10.1007/JHEP10(2012)081, arXiv:1207.2159.

[63] B. Fuks, M. Klasen, D. R. Lamprea, and M. Rothering, "Precision predictions for electroweak superpartner production at hadron colliders with Resummino", *Eur. Phys. J. C* **73** (2013) 2480, doi:10.1140/epjc/s10052-013-2480-0, arXiv:1304.0790.

[64] M. Krämer et al., "Supersymmetry production cross sections in pp collisions at $\sqrt{s} = 7$ TeV", (2012). arXiv:1206.2892.

[65] P. Meade and M. Reece, "BRIDGE: branching ratio inquiry / decay generated events", (2007). arXiv:hep-ph/0703031.

[66] J. Pumplin et al., "New generation of parton distributions with uncertainties from global QCD analysis", *JHEP* **07** (2002) 012, doi:10.1088/1126-6708/2002/07/012, arXiv:hep-ph/0201195.

[67] P. M. Nadolsky et al., "Implications of CTEQ global analysis for collider observables", *Phys. Rev. D* **78** (2008) 013004, doi:10.1103/PhysRevD.78.013004, arXiv:0802.0007.

[68] S. Heinemeyer et al., "Handbook of LHC Higgs cross sections: 3. Higgs properties", (2013). arXiv:1307.1347.

[69] CMS Collaboration, "Photon reconstruction and identification at $\sqrt{s} = 7$ TeV", CMS Physics Analysis Summary CMS-PAS-EGM-10-005, 2010.

[70] CMS Collaboration, "Energy calibration and resolution of the CMS electromagnetic calorimeter in pp collisions at $\sqrt{s} = 7$ TeV", *JINST* **8** (2013) P09009, doi:10.1088/1748-0221/8/09/P09009, arXiv:1306.2016.

[71] CMS Collaboration, "Photon ID performance with 19.6 fb^{-1} of data collected at $\sqrt{s} = 8$ TeV with the CMS detector", CMS Detector Performance Note CMS-DP-2013-010, 2013.

[72] C. G. Lester and D. J. Summers, "Measuring masses of semi-invisibly decaying particle pairs produced at hadron colliders", *Phys. Lett. B* **463** (1999) 99, doi:10.1016/S0370-2693(99)00945-4, arXiv:hep-ph/9906349.

[73] A. Barr, C. G. Lester, and P. Stephens, "A variable for measuring masses at hadron colliders when missing energy is expected; m_{T2}: the truth behind the glamour", *J. Phys. G* **29** (2003) 2343, doi:10.1088/0954-3899/29/10/304, arXiv:hep-ph/0304226.

[74] CMS Collaboration, "Search for physics beyond the standard model in events with a Z boson, jets, and missing transverse energy in pp collisions at $\sqrt{s} = 7$ TeV", *Phys. Lett. B* **716** (2012) 260, doi:10.1016/j.physletb.2012.08.026, arXiv:1204.3774.

[75] A. D. Martin, W. J. Stirling, R. S. Thorne, and G. Watt, "Parton distributions for the LHC", *Eur. Phys. J. C* **63** (2009) 189, doi:10.1140/epjc/s10052-009-1072-5, arXiv:0901.0002.

[76] R. D. Ball et al., "Impact of heavy quark masses on parton distributions and LHC phenomenology", *Nucl. Phys. B* **849** (2011) 296, doi:10.1016/j.nuclphysb.2011.03.021, arXiv:1101.1300.

[77] M. Botje et al., "The PDF4LHC working group interim recommendations", (2011). arXiv:1101.0538.

[78] CMS Collaboration, "CMS luminosity based on pixel cluster counting – summer 2013 update", CMS Physics Analysis Summary CMS-PAS-LUM-13-001, 2013.

[79] A. L. Read, "Presentation of search results: the CL_S technique", *J. Phys. G* **28** (2002) 2693, doi:10.1088/0954-3899/28/10/313.

[80] T. Junk, "Confidence level computation for combining searches with small statistics", *Nucl. Instr. and Meth. A* **434** (1999) 435, doi:10.1016/S0168-9002(99)00498-2, arXiv:hep-ex/9902006.

[81] ATLAS and CMS Collaborations, "Procedure for the LHC Higgs boson search combination in Summer 2011", Technical Report CMS-NOTE-2011-005, ATL-PHYS-PUB-2011-11, 2011.

A Additional results

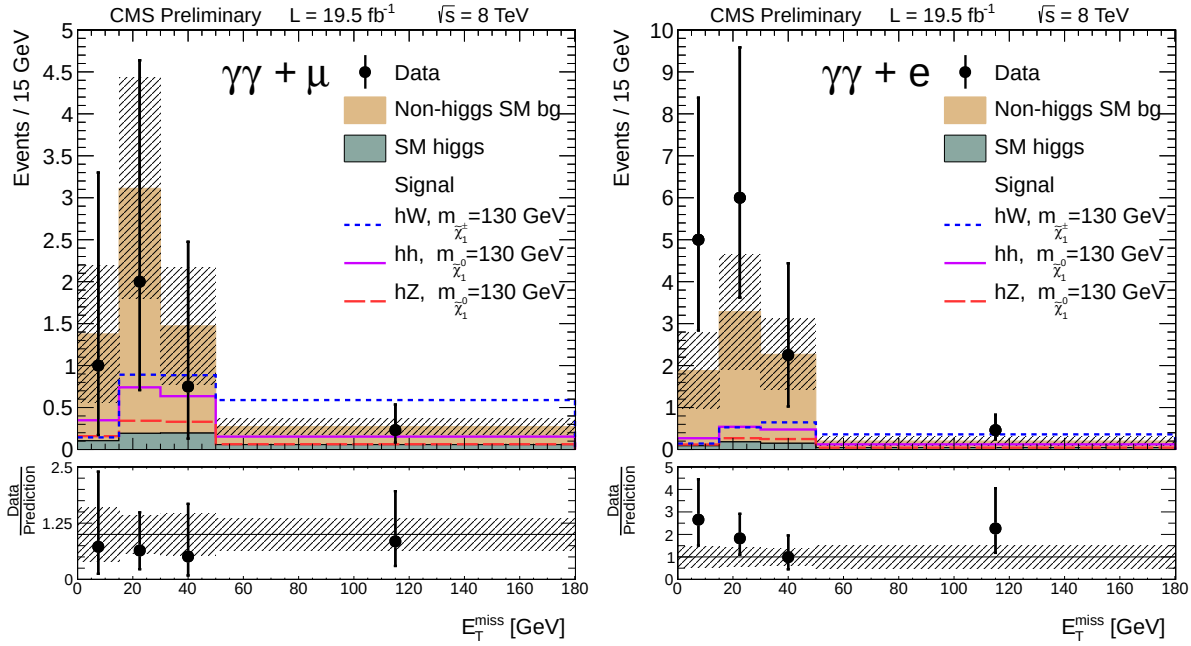

Figure 19: Observed numbers of events as a function of $E_{\mathrm{T}}^{\mathrm{miss}}$ for the hh, hZ, and hW $\rightarrow$ $\gamma\gamma$+leptons analysis of Section 6.3, in comparison with the (stacked) SM background estimates, for the (left) muon and (right) electron samples. The hatched bands show the total uncertainty of the background prediction, with statistical and systematic terms combined. The (unstacked) results for various signal scenarios are also shown. For the hh and hZ scenarios, the higgsino mass is 130 GeV and the LSP (gravitino) mass is 1 GeV. For the hW scenario, $\mathrm{m}_{\tilde{\chi}_2^0} = \mathrm{m}_{\tilde{\chi}_1^\pm} = 130\,\mathrm{GeV}$ and $m_{\tilde{\chi}_1^0} = 1\,\mathrm{GeV}$.

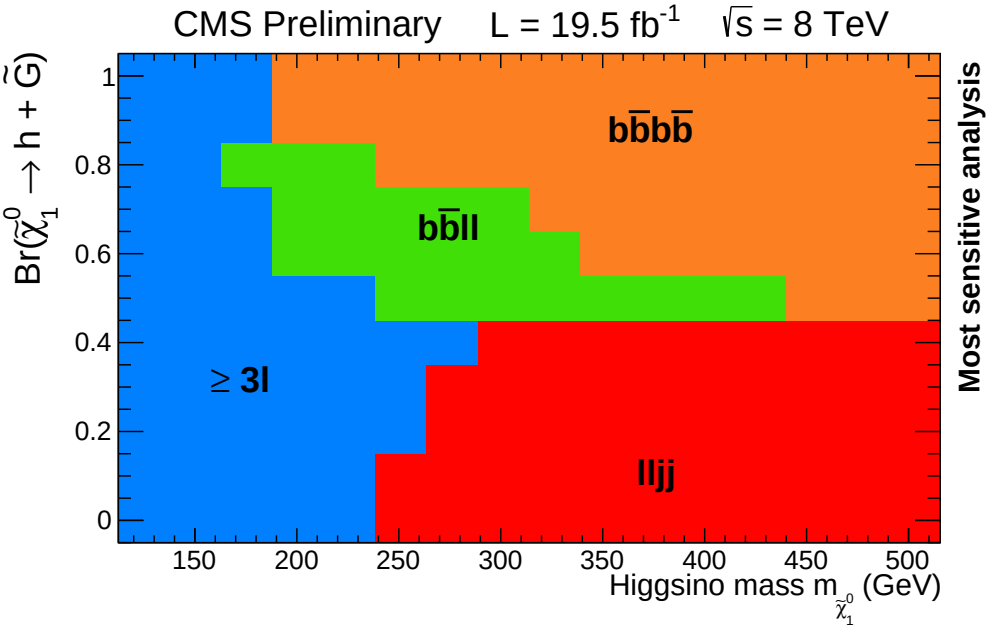

Figure 20: The search channel that provides the most stringent 95% CL upper limit on $\widetilde{\chi}_1^0$ higgsino pair production in the plane of the higgsino branching fraction to a Higgs boson and the LSP, versus the higgsino mass.

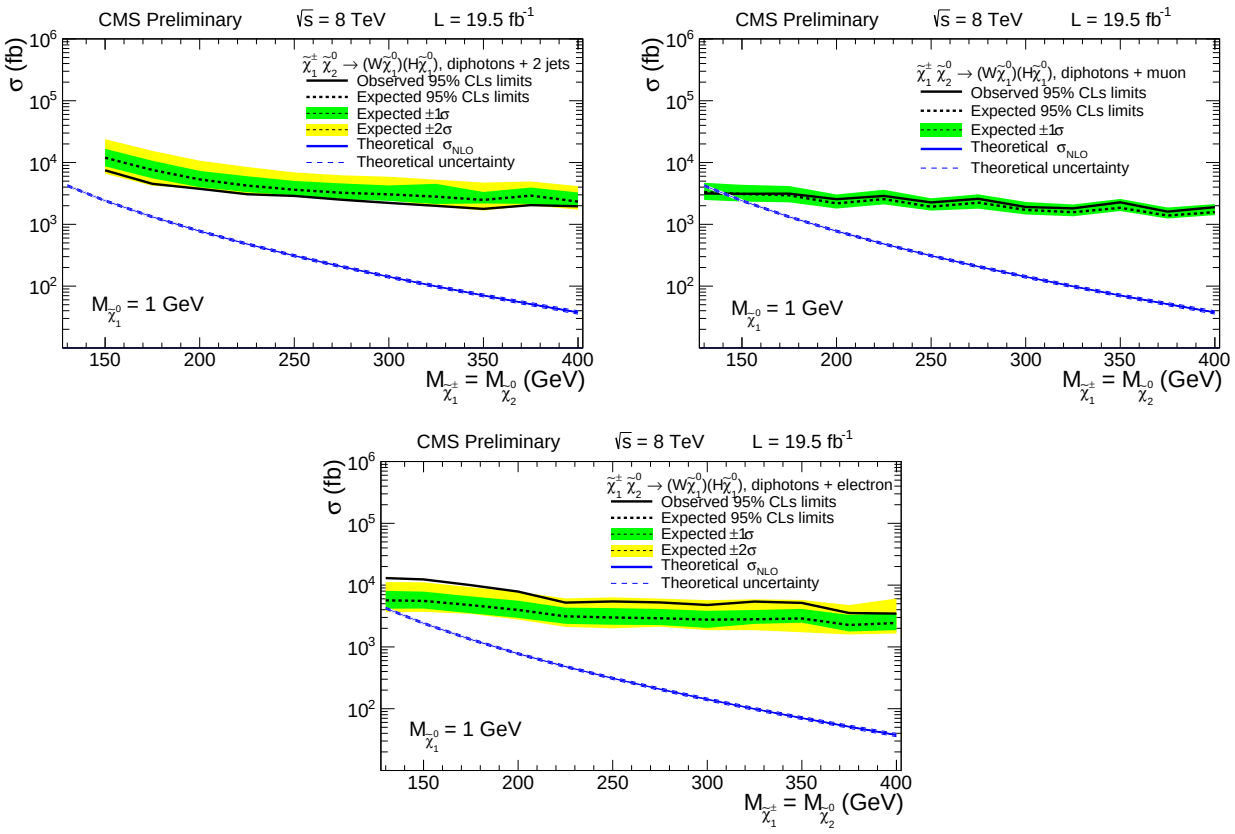

Figure 21: Observed and expected 95% confidence level (CL) upper limits on the cross section for chargino-neutralino $\widetilde{\chi}_1^{\pm}\widetilde{\chi}_2^0$ pair production (with $m_{\widetilde{\chi}_1^{\pm}} = m_{\widetilde{\chi}_2^0}$) as a function of the $\widetilde{\chi}_2^0$ mass assuming an LSP mass of 1 GeV, for (top left) the $\gamma\gamma$+2 jets study of Section 6.2, and (top right and bottom), the $\gamma\gamma$+leptons studies (for the muon and electron samples, respectively) of Section 6.3. The green and yellow bands indicate the one- and two-standard-deviation uncertainty intervals, respectively. The theoretical cross section is also shown.

B Event selection flow tables

In this appendix, we present tables that illustrate the event selection process, or "flow", for the analyses presented in Sections 5–7. For each analysis, the selection flow is illustrated for two or more signal points. These tables are intended as an aid for those wishing to replicate these analyses using signal scenarios other than those considered in the present work.

Table 8: Number of signal events remaining after each stage of the event selection for the $\mathrm{hh} \to \mathrm{b\bar{b}b\bar{b}}$ search, with a higgsino mass of 250 GeV and an LSP (gravitino) mass of 1 GeV. The results are normalized to an integrated luminosity of 19.3 fb^{-1} using NLO+NLL calculations. The uncertainties are statistical. "$\mathcal{S}_{\mathrm{MET}}$ bin 0" corresponds to $0 < \mathcal{S}_{\mathrm{MET}} < 30$. The baseline selection accounts for the primary vertex criteria and for quality requirements applied to the $E_{\mathrm{T}}^{\mathrm{miss}}$ distribution. This search is described in Section 5.

hh events, $m_{\tilde{\chi}_1^0} = 250\,\mathrm{GeV}$	$\mathcal{S}_{\mathrm{MET}}$ bin 0	$\mathcal{S}_{\mathrm{MET}}$ bin 1	$\mathcal{S}_{\mathrm{MET}}$ bin 2	$\mathcal{S}_{\mathrm{MET}}$ bin 3	$\mathcal{S}_{\mathrm{MET}}$ bin 4
All events	590 ± 2	264 ± 2	376 ± 2	107 ± 1	22.7 ± 0.5
Baseline selection	548 ± 2	257 ± 2	369 ± 2	106 ± 1	22.1 ± 0.5
$p_{\mathrm{T}} > 50\,\mathrm{GeV}$, leading 2 jets	470 ± 2	220 ± 1	321 ± 2	95 ± 1	20.7 ± 0.5
Number of jets = 4 or 5	288 ± 2	132 ± 1	196 ± 1	58.3 ± 0.8	12.2 ± 0.4
Lepton vetoes	280 ± 2	128 ± 1	190 ± 1	56.7 ± 0.8	11.7 ± 0.4
Isolated track veto	253 ± 2	116 ± 1	173 ± 1	51.9 ± 0.7	10.8 ± 0.3
$\Delta\phi_{\mathrm{min}}$ requirement	111 ± 1	64.3 ± 0.8	133 ± 1	42.6 ± 0.7	9.1 ± 0.3
3b selection	15.3 ± 0.4	8.6 ± 0.3	19.0 ± 0.4	6.3 ± 0.3	1.3 ± 0.1
$\Delta R_{\mathrm{max}} < 2.2$	6.6 ± 0.3	3.4 ± 0.2	7.6 ± 0.3	2.5 ± 0.2	0.53 ± 0.08
Higgs boson SIG region	2.7 ± 0.2	1.3 ± 0.1	2.7 ± 0.2	0.87 ± 0.10	0.14 ± 0.04
Trigger emulation	0.41 ± 0.06	0.83 ± 0.08	2.3 ± 0.1	0.82 ± 0.09	0.13 ± 0.04
4b selection	20.3 ± 0.5	12.3 ± 0.4	26.3 ± 0.5	8.4 ± 0.3	1.7 ± 0.1
$\Delta R_{\mathrm{max}} < 2.2$	9.8 ± 0.3	5.9 ± 0.2	11.6 ± 0.3	3.6 ± 0.2	0.79 ± 0.09
Higgs boson SIG region	4.7 ± 0.2	3.0 ± 0.2	5.1 ± 0.2	1.5 ± 0.1	0.30 ± 0.06
Trigger emulation	0.55 ± 0.07	1.8 ± 0.1	4.4 ± 0.2	1.4 ± 0.1	0.28 ± 0.05

Table 9: Number of signal events remaining after each stage of the event selection for the $hh \to b\bar{b}b\bar{b}$ search, with a higgsino mass of 400 GeV and an LSP (gravitino) mass of 1 GeV. The results are normalized to an integrated luminosity of 19.3 fb^{-1} using NLO+NLL calculations. The uncertainties are statistical. "$\mathcal{S}_{MET}$ bin 0" corresponds to $0 < \mathcal{S}_{MET} < 30$. The baseline selection accounts for the primary vertex criteria and for quality requirements applied to the E_T^{miss} distribution. This search is described in Section 5.

hh events, $m_{\tilde{\chi}_1^0} = 400$ GeV	$\mathcal{S}_{MET}$ bin 0	$\mathcal{S}_{MET}$ bin 1	$\mathcal{S}_{MET}$ bin 2	$\mathcal{S}_{MET}$ bin 3	$\mathcal{S}_{MET}$ bin 4
All events	28.8 ± 0.3	15.9 ± 0.2	35.3 ± 0.3	31.1 ± 0.3	51.9 ± 0.4
Baseline selection	26.9 ± 0.3	15.6 ± 0.2	34.6 ± 0.3	30.5 ± 0.3	50.9 ± 0.4
$p_T > 50$ GeV, leading 2 jets	25.3 ± 0.2	14.6 ± 0.2	32.4 ± 0.3	28.8 ± 0.3	49.3 ± 0.3
Number of jets = 4 or 5	15.7 ± 0.2	9.1 ± 0.1	19.8 ± 0.2	17.6 ± 0.2	30.4 ± 0.3
Lepton vetoes	15.3 ± 0.2	8.8 ± 0.1	19.3 ± 0.2	17.1 ± 0.2	29.8 ± 0.3
Isolated track veto	13.9 ± 0.2	8.0 ± 0.1	17.6 ± 0.2	15.6 ± 0.2	27.3 ± 0.3
$\Delta\phi_{min}$ requirement	5.9 ± 0.1	4.25 ± 0.10	13.3 ± 0.2	12.9 ± 0.2	24.4 ± 0.2
3b selection	0.85 ± 0.04	0.56 ± 0.04	1.90 ± 0.07	1.70 ± 0.06	3.64 ± 0.09
$\Delta R_{max} < 2.2$	0.44 ± 0.03	0.31 ± 0.03	1.03 ± 0.05	0.91 ± 0.05	2.12 ± 0.07
Higgs boson SIG region	0.22 ± 0.02	0.13 ± 0.02	0.45 ± 0.03	0.30 ± 0.03	0.88 ± 0.05
Trigger emulation	0.029 ± 0.007	0.09 ± 0.01	0.39 ± 0.03	0.29 ± 0.03	0.83 ± 0.04
4b selection	1.18 ± 0.05	0.85 ± 0.04	2.44 ± 0.08	2.57 ± 0.08	4.6 ± 0.1
$\Delta R_{max} < 2.2$	0.77 ± 0.04	0.52 ± 0.04	1.40 ± 0.06	1.59 ± 0.06	3.02 ± 0.09
Higgs boson SIG region	0.45 ± 0.03	0.29 ± 0.03	0.77 ± 0.04	0.83 ± 0.04	1.56 ± 0.06
Trigger emulation	0.07 ± 0.01	0.20 ± 0.02	0.68 ± 0.04	0.78 ± 0.04	1.47 ± 0.06

Table 10: Number of signal events remaining after each stage of the event selection for the $hh \to \gamma\gamma b\bar{b}$ search, described in Section 6.1, and for the hZ and hW $\to \gamma\gamma$+2 jets search, described in Section 6.2. The hh and hZ scenarios assume a higgsino mass value of 130 GeV and an LSP (gravitino) mass of 1 GeV. For the hW scenario, $m_{\tilde{\chi}_1^\pm} = m_{\tilde{\chi}_2^0} = 130$ GeV and the LSP ($\tilde{\chi}_1^0$) mass is 1 GeV. The results are normalized to an integrated luminosity of 19.7 fb^{-1} using NLO+NLL calculations for the hh and hZ results and NLO calculations for the hW results. The uncertainties are statistical.

	hh events	hZ events	hW events
All events	71.5 ± 0.4	63.3 ± 0.3	118 ± 1
Trigger emulation	53.6 ± 0.4	48.3 ± 0.2	89.9 ± 0.4
Photon selection (except for η requirement)	34.0 ± 0.3	30.9 ± 0.2	57.2 ± 0.4
$120 < m_{\gamma\gamma} < 131$ GeV	31.1 ± 0.3	28.0 ± 0.2	51.9 ± 0.3
$\lvert\eta\rvert < 1.4442$ for photons	20.0 ± 0.2	17.9 ± 0.1	32.9 ± 0.3
Lepton vetoes	4.1 ± 0.1	16.7 ± 0.1	27.5 ± 0.2
Reject events with $95 < m_{b\bar{b}} < 155$ GeV	—	7.7 ± 0.1	13.0 ± 0.2
$70 < m_{jj} < 110$ GeV	—	4.6 ± 0.1	7.9 ± 0.1
Exactly two b jets	4.1 ± 0.1	—	—
$95 < m_{b\bar{b}} < 155$ GeV	3.5 ± 0.1	—	—

Table 11: Number of signal events remaining after each stage of the event selection for the hh and hW $\rightarrow \gamma\gamma$+leptons searches. The hh scenario assumes a higgsino mass value of 130 GeV and an LSP (gravitino) mass of 1 GeV. For the hW scenario, $m_{\widetilde{\chi}_1^\pm} = m_{\widetilde{\chi}_2^0} = 130$ GeV and the LSP ($\widetilde{\chi}_1^0$) mass is 1 GeV. The results are normalized to an integrated luminosity of 19.5 fb^{-1} using NLO+NLL calculations for the hh results and NLO calculations for the hW results. The uncertainties are statistical. The baseline selection accounts for the primary vertex criteria and for quality requirements applied to the E_T^{miss} distribution. This search is described in Section 6.3.

	hh events		hW events	
	$\gamma\gamma$+muon	$\gamma\gamma$+electron	$\gamma\gamma$+muon	$\gamma\gamma$+electron
All events	90.3 ± 0.6	90.3 ± 0.6	261 ± 1	261 ± 1
Baseline selection	90.3 ± 0.6	90.3 ± 0.6	261 ± 1	261 ± 1
Trigger emulation	70.7 ± 0.5	70.7 ± 0.5	200 ± 1	200 ± 1
Photon selection	27.4 ± 0.3	27.4 ± 0.3	77.8 ± 0.6	77.8 ± 0.6
Lepton selection	3.5 ± 0.1	3.8 ± 0.1	7.1 ± 0.2	7.6 ± 0.2
At most one b jet	3.5 ± 0.1	3.8 ± 0.1	7.1 ± 0.2	7.6 ± 0.2
$\Delta R(\gamma, \text{lepton}) > 0.3$	3.5 ± 0.1	3.7 ± 0.1	7.1 ± 0.2	7.6 ± 0.2
Reject events with $86 < m_{e\gamma} < 96$ GeV	3.5 ± 0.1	2.6 ± 0.1	7.1 ± 0.2	5.1 ± 0.2
$120 < m_{\gamma\gamma} < 131$ GeV	3.3 ± 0.1	2.5 ± 0.1	6.8 ± 0.2	4.7 ± 0.2

Table 12: Number of signal events remaining after each stage of the event selection for the hZ search with h $\rightarrow b\bar{b}$ and Z $\rightarrow \ell^+\ell^-$, with higgsino mass values of 130 and 200 GeV and an LSP (gravitino) mass of 1 GeV. The results are normalized to an integrated luminosity of 19.5 fb^{-1} using NLO+NLL calculations. The uncertainties are statistical. The baseline selection accounts for the primary vertex criteria and for quality requirements applied to the E_T^{miss} distribution. This search is described in Section 7.

	$m_{\widetilde{\chi}_1^0} = 130$ GeV			$m_{\widetilde{\chi}_1^0} = 200$ GeV		
hZ events	ee	$\mu\mu$	ee + $\mu\mu$	ee	$\mu\mu$	ee + $\mu\mu$
Baseline selection	579 ± 2	576 ± 2	1154 ± 2	100 ± 1	102 ± 1	202 ± 1
Trigger emulation	548 ± 1	494 ± 1	1042 ± 2	95.5 ± 0.6	87.2 ± 0.5	183 ± 1
Lepton ID & isolation	262 ± 1	315 ± 1	577 ± 1	50.0 ± 0.4	60.9 ± 0.5	111 ± 1
2 leptons ($p_T > 20$ GeV)	238 ± 1	287 ± 1	525 ± 1	47.2 ± 0.4	57.3 ± 0.4	105 ± 1
$81 < m_{\ell\ell} < 101$ GeV	231 ± 1	277 ± 1	507 ± 1	45.7 ± 0.4	55.3 ± 0.4	101 ± 1
3rd lepton veto	230 ± 1	276 ± 1	505 ± 1	45.5 ± 0.4	55.1 ± 0.4	101 ± 1
Hadronic τ-lepton veto	226 ± 1	271 ± 1	496 ± 1	44.8 ± 0.4	54.3 ± 0.4	99.1 ± 0.5
≥ 2 jets	148 ± 1	176 ± 1	323 ± 1	31.0 ± 0.3	37.5 ± 0.3	68.5 ± 0.4
≥ 2 b-tagged jets	44.1 ± 0.4	51.1 ± 0.4	95.2 ± 0.6	9.2 ± 0.2	11.1 ± 0.2	20.3 ± 0.3
$100 < m_{b\bar{b}} < 150$ GeV	34.6 ± 0.3	40.0 ± 0.3	74.6 ± 0.5	7.2 ± 0.2	8.7 ± 0.2	15.9 ± 0.3
$M_{T2}^j > 200$ GeV	7.6 ± 0.1	8.4 ± 0.1	16.0 ± 0.1	3.0 ± 0.1	3.3 ± 0.1	6.3 ± 0.1
$E_T^{miss} > 60$ GeV	2.6 ± 0.1	2.8 ± 0.1	5.4 ± 0.1	2.2 ± 0.1	2.5 ± 0.1	4.7 ± 0.1
$E_T^{miss} > 80$ GeV	1.5 ± 0.1	1.6 ± 0.1	3.1 ± 0.1	2.0 ± 0.1	2.2 ± 0.1	4.2 ± 0.1
$E_T^{miss} > 100$ GeV	0.8 ± 0.1	0.9 ± 0.1	1.7 ± 0.1	1.6 ± 0.1	1.7 ± 0.1	3.3 ± 0.1